

## RESEARCH ARTICLE

10.1002/2017GC007100

## Key Points:

- A Holocene to Oligocene tephrostratigraphy has been developed for IBM and Japan tephra
- At least three major phases of highly explosive volcanism during Oligocene to Pleistocene time with variable sources from Japan and IBM arcs
- Assigning source regions and volume estimates for IBM eruptions and refining eruptive volumes for 12 correlated Japanese eruptions

## Supporting Information:

- Supporting Information S1
- Table S1
- Table S2
- Table S3
- Table S4

## Correspondence to:

S. Kutterolf,  
skutterolf@geomar.de

## Citation:

Kutterolf, S., Schindlbeck, J. C., Robertson, A. H. F., Avery, A., Baxter, A. T., Petronotis, K., & Wang, K.-L. (2018). Tephrostratigraphy and provenance from IODP Expedition 352, Izu-Bonin arc: Tracing tephra sources and volumes from the Oligocene to recent. *Geochemistry, Geophysics, Geosystems*, 19, 150–174. <https://doi.org/10.1002/2017GC007100>

Received 5 JUL 2017

Accepted 15 NOV 2017

Accepted article online 7 DEC 2017

Published online 20 JAN 2018

## Tephrostratigraphy and Provenance From IODP Expedition 352, Izu-Bonin Arc: Tracing Tephra Sources and Volumes From the Oligocene to Recent

S. Kutterolf<sup>1</sup>, J. C. Schindlbeck<sup>1,2</sup>, A. H. F. Robertson<sup>3</sup>, A. Avery<sup>4</sup>, A. T. Baxter<sup>5</sup>, K. Petronotis<sup>6</sup>, and K.-L. Wang<sup>7,8</sup>
<sup>1</sup> FB4, Dynamics of the Ocean Floor, GEOMAR Helmholtz Center for Ocean Research Kiel, Kiel, Germany, <sup>2</sup> Heidelberg University, Institute of Earth Sciences, Heidelberg, Germany, <sup>3</sup> School of GeoSciences, University of Edinburgh, Edinburgh, UK, <sup>4</sup> Earth, Ocean and Atmospheric Sciences, Florida State University, Tallahassee, FL, USA, <sup>5</sup> School of Environmental and Rural Science, University of New England, Armidale, NSW, Australia, <sup>6</sup> International Ocean Discovery Program, Texas A&M University, College Station, TX, USA, <sup>7</sup> Institute of Earth Sciences, Academia Sinica, Taipei, Taiwan, <sup>8</sup> Department of Geosciences, National Taiwan University, Taipei, Taiwan

**Abstract** Provenance studies of widely distributed tephra, integrated within a well-defined temporal framework, are important to deduce systematic changes in the source, scale, distribution, and changes in regional explosive volcanism. Here, we establish a robust tephrostratigraphy for a total of 157 marine tephra layers collected during IODP Expedition 352. We infer at least three major phases of highly explosive volcanism during Oligocene to Pleistocene time. Provenance analysis based on glass composition assigns 56 of the tephra to a Japan source, including correlations with 12 major and widespread tephra layers resulting from individual eruptions in Kyushu, Central Japan, and North Japan between 115 ka and 3.5 Ma. The remaining 101 tephra are assigned to four source regions along the Izu-Bonin arc. One, exclusively assigned to the Oligocene age, is proximal to the Bonin Ridge islands; two reflect eruptions within the volcanic front and back-arc of the central Izu-Bonin arc, and a fourth region corresponds to the Northern Izu-Bonin arc source. First-order volume estimates imply eruptive magnitudes ranging from 6.3 to 7.6 for Japan-related eruptions and between 5.5 and 6.5 for IBM eruptions. Our results suggest tephra between 30 and 22 Ma reflect a subtly different Izu-Bonin chemical signature compared to the recent arc. After a ~9 Ma gap in eruption, tephra supply from the Izu-Bonin arc predominated from 15 to 5 Ma, and finally a subequal mixture of tephra sources from the (palaeo)Honshu and Izu-Bonin arcs occurred within the last ~5 Ma.

**Plain Language Summary** Provenance studies of widely distributed tephra, integrated within a well-defined temporal framework, are important to deduce systematic changes in the source, scale, distribution, and changes in regional explosive volcanism. Here, we establish a robust tephrostratigraphy for marine tephra layers collected during IODP Expedition 352, assigning the eruptions to both sources from the Japan mainland and the Izu-Bonin arc. Using correlations with individual eruptions in Japan, we have also estimated respective eruptive volumes and eruption magnitudes. Together with marine tephra assigned to provenance regions within the Izu-Bonin arc system, this indicates for the first time how large eruptions from the source regions must have been in the past in this region. The tephra record additionally provides glimpses of the history of explosive volcanism on the Izu-Bonin arc system back to the Oligocene and also helps to indicate how this relates to explosive volcanism in Japan.

## 1. Introduction

Highly explosive eruptions and their related products in the deep sea are integral to arc volcanism, particularly in ocean-ocean subduction zone settings where subaerial outcrops are sparse or absent. At convergent margins, ash layers are well preserved in marine and lacustrine-depositing environments where they may provide detailed records of explosive volcanism over long-time periods (Carey, 2000; Carey & Sigurdsson, 2000; Keller et al., 1978; Kutterolf et al., 2008b; Ledbetter, 1985; Schindlbeck et al., 2016a, 2016b). Ash layers represent excellent stratigraphic marker beds in marine sediment sequences owing to their widespread distribution, potentially variable facies, near-instantaneous emplacement, distinctive and correlative chemical

© 2017. The Authors.

This is an open access article under the terms of the Creative Commons Attribution License, which permits use, distribution and reproduction in any medium, provided the original work is properly cited.

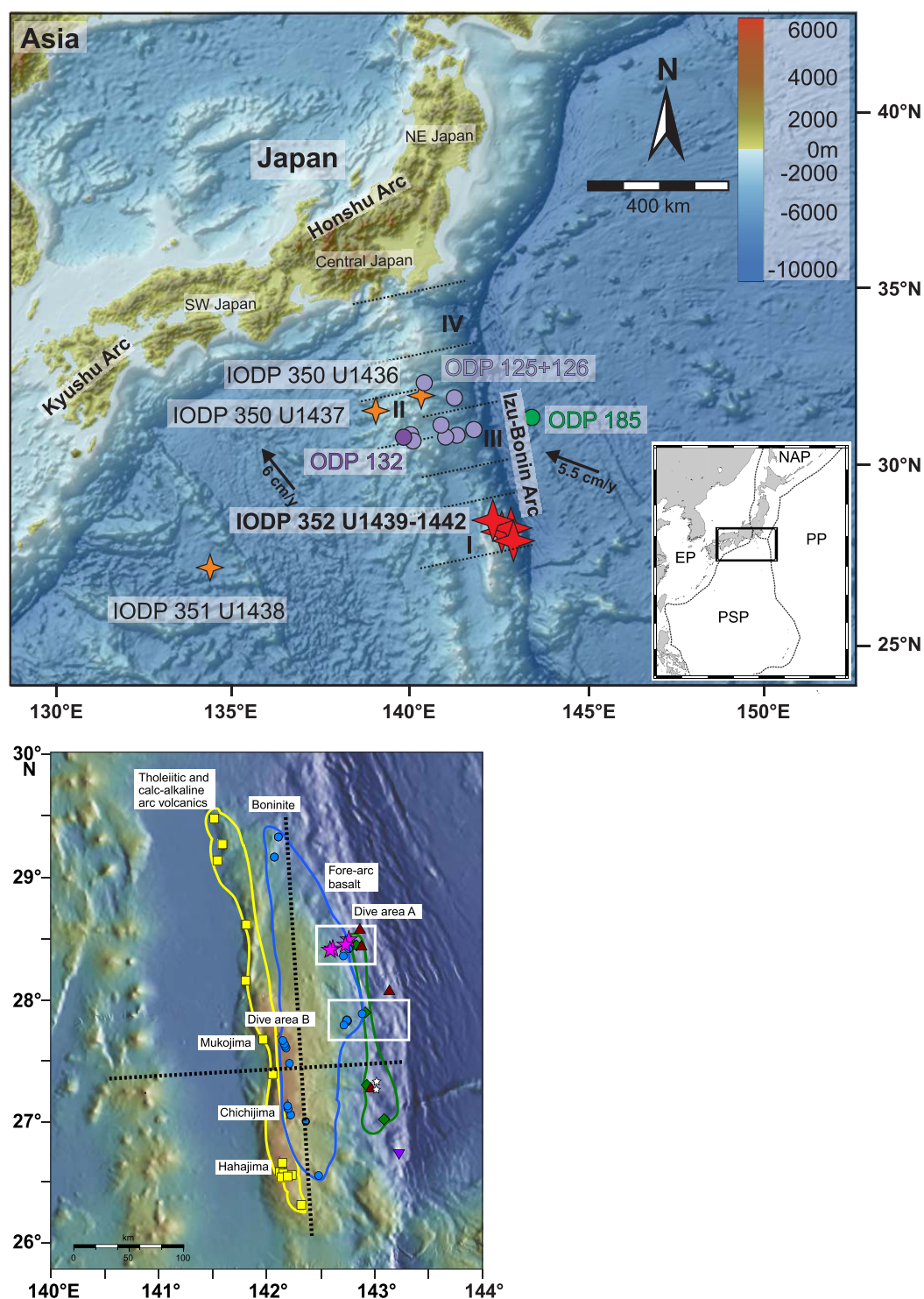


**Figure 1.** Overview bathymetry of the Japan-Izu-Bonin region (<http://www.geomapapp.org>; GMRT-Global Multi-Resolution Topography; Ryan et al., 2009) including borehole positions of IODP Expedition 350–351 (orange stars) and 352 (red stars), and also ODP cruises (green and violet circles). Arrows indicate convergence direction and rate between the Philippine Sea plate and Japan and also the Pacific plate and the Philippine Sea plate (Miller et al., 2006). Dashed lines and roman numerals represent potential IBM source regions of the marine tephras. Inset shows the location of main map. EP, Eurasian plate; PP, Pacific plate; PSP, Philippine Sea plate; and NAP, North American plate.

signatures, and the presence of phenocrysts suitable for radiometric dating (e.g., Kutterolf et al., 2008a, 2008b, 2008c, 2008d). Such sediments can also provide constraints on the temporal evolution of both the volcanic source region and the ash-bearing sediment facies (Schindlbeck et al., 2016c; Scudder et al., 2016). In the forearc setting investigated here, tephra layers and intercalated volcanoclastic sediments are compositionally variable and so can provide important temporal and spatial information concerning volcanism in several geographically separate arc systems.

The Izu-Bonin-Mariana (IBM) system holds the key to understanding the formation of oceanic crust immediately following subduction initiation at around 50 Ma (Bloomer et al., 1995; Cosca et al., 1998; Stern, 2004). Subsequent subduction lead to the onset of typical calc-alkaline arc volcanism <45 Ma (Ishizuka et al., 2011, 2006). Marine tephra recovered from sediment cores and dredge samples help to document the regional arc development. The suprasubduction zone crust of the IBM system is overlain by an exceptionally intact and mostly unaltered, mainly volcanogenic sequence, which reflects regional calc-alkaline arc volcanism (Pearce et al., 2013) and provides the basis of this study.

Several ODP (Ocean Drilling Program) expeditions (Legs 125, 126, 132, 185; Figure 1) have explored the IBM forearc and used the geochemistry of sediments and volcanic deposits as an indication of local to regional-scale arc magmatism, tectonic development, and subduction-related processes (e.g., Gill et al., 1994; Straub, 2008; Straub et al., 2010, 2004). International Ocean Discovery Program (IODP) Expeditions 350, 351, 352 (Figure 1), which comprise the IBM project, took place during 2014.

In this paper, we will establish detailed and accurate correlations between marine ash beds that were recovered from four IBM forearc drill sites during IODP Expedition 352. We utilize a large set of major and trace element chemical data for ash samples to identify potential source volcanoes in the IBM and Japan arc systems, while taking into account age constraints provided by biostratigraphy and paleomagnetism. Our results provide a reference tephrochronostratigraphy for the wider IBM/Japan region, refine shipboard age models for the drill sites, allow insights into the evolution of explosive arc volcanism from the Oligocene onwards, and support palaeogeographic and palaeotectonic interpretations of the background hemipelagic sediments (Robertson et al., 2017).

## 2. Geological Background

The modern IBM arc extends over 2,800 km, from the Izu Peninsula (Japan) in the north, where it is currently colliding with the Honshu arc (Japan), as far as Guam (USA) in the south. The arc formed by subduction of the Pacific Plate beneath the eastern margin of the Philippine Sea Plate in the Western Pacific (Figure 1), beginning ~50 Ma ago (e.g., Stern et al., 2003). The IBM subduction zone has a multiphase history including back-arc spreading (~30 to ~15 Ma), formation of marginal basins (e.g., Shikoku Basin), amalgamation to the Honshu arc of Japan mainland, and also episodes of volcanic quiescence and reactivation (Arima & Stern, 1997; Müller et al., 2016; Stern et al., 2003; Wu et al., 2016; Yamazaki & Stern, 1997).

The initial phase of subduction around 50 Ma was associated with the westward subduction of the Pacific Plate beneath the eastern margin of the Philippine Sea Plate (Hochstaedter et al., 2001; Taylor, 1992). A reorganization of plate boundaries throughout the Pacific is proposed around this time (Hall, 2002; Hall et al., 2003; Okino et al., 2004; Whittaker et al., 2007). During subduction initiation (~52–47 Ma), igneous activity produced MORB-like forearc basalts ("FAB") (Reagan et al., 2010), low-Ca boninites, low-K tholeiitic to calc-alkaline arc basalts, and subordinate low-K rhyodacite within the subsequent forearc area. Typical arc and rear-arc volcanism, represented by the Kyushu-Palau arc, was initiated during the Eocene to Oligocene, shedding volcanic material into the modern IBM forearc (Ishizuka et al., 2011, 2006; Reagan et al., 2017; Ryan et al., 2017; Taylor, 1992).

At around 25 Ma, rifting along the length of the Kyushu-Palau arc opened the Shikoku Basin, splitting former rear-arc and arc-front volcanoes. The northerly IBM arc-front magmatism declined or ceased during opening of the Shikoku Basin but resumed as basaltic to dacitic magmatism (at ~17 Ma) within the Izu rear-arc area (eastward of the arc) at ~15 Ma, slightly west of its Eocene to Oligocene position (Ishizuka et al., 2011; Taylor, 1992). Rear-arc magmatism subsequently migrated ENE toward the arc front, producing a series of large seamounts until ~3 Ma. The Quaternary Izu volcanic front was constructed on ~20 km-thick

crust (Suyehrio et al., 1996). The subducting slab is composed of basaltic crust of inferred Jurassic age, covered by ~400 m-thick Mesozoic and Cenozoic pelagic sediments including arc-derived ash (Plank, 2001).

### 3. Explosive Volcanism From Japan and IBM Arcs

Explosive subduction-related volcanism is reported from the IBM arc as early as the Eocene/Oligocene boundary (Arculus et al., 2015; Reagan et al., 2015), and from the (Paleo-) Honshu, Ryukyu-Kyushu, and IBM arcs at least since the Miocene (Ito et al., 1989; Nakajima et al., 1995; Sato, 1994; Taylor et al., 1992; Yamamoto, 1992).

#### 3.1. Quaternary Explosive Volcanism

The volcanoes of the Honshu arc that formed by subduction of the Pacific Plate and/or the Philippine Sea Plate beneath the Eurasian Plate (Figure 1), are known for large-scale explosive eruptions (Machida, 1999). Of the 16 Quaternary calderas recognized on Honshu, the majority are located in central and northern Honshu (Machida, 1999), with only two in southwest Honshu. A tephrostratigraphy has been established for 80 widespread tephra layers of Quaternary to Late Pliocene age, in and around Japan (Kimura et al., 2015; Machida, 1999, 2002). The northern part of Honshu is characterized by caldera-forming eruptions, whereas the central to western volcanic centers on Honshu and the IBM arc are typified by stratovolcanoes, only some of which are associated with caldera formation (Machida, 1999).

Quaternary volcanism of the northern Izu-Bonin arc comprises 8 submarine calderas and 11 island volcanoes (Tamura et al., 2005). Volcanism is generally bimodal with basalt and volumetrically dominant island volcanoes, as well as rhyolite-dominant calderas (e.g., Tamura & Tatsumi, 2002). Volcanic intensity at the IBM arc increased around 2 Ma and became strongly rhyolitic before second-stage backarc rifting began (Gill et al., 1994).

#### 3.2. Neogene Volcanism

Based on available evidence from sparse subaerial outcrops and ocean drilling data, a significant increase in explosive volcanism appears to be occurred within the frontal arc, backarc, and forearc areas of the Izu-Bonin arc at around 17 Ma (Taylor et al., 1992).

Previous studies (Ito et al., 1989; Sato, 1994; Yamamoto, 1992) suggested that caldera-forming felsic volcanism in the NE Japan arc began at ~13 Ma in response to increased rate of subduction of the Pacific Plate beneath the North American Plate, including Japan (Figure 1). Caldera volcanoes cluster every 40–80 km along the main part of the arc in NE Honshu where six Neogene centers existed, each comprising 3 to >10 calderas (Yamamoto, 2009). Most of the caldera-forming eruptions took place during the early Late Miocene to Pliocene volcanic phase (Acocella et al., 2008). Ten widespread tephra layers are identified in central Japan within the Plio-Pleistocene Hokuriki Group (Tamura & Yamazaki, 2004). This data set is complemented by geochemical characterization of 17 Late Pliocene tephras from caldera-forming eruptions of the (Paleo-) Honshu arc (Kimura et al., 2015, Satoguchi & Nagahashi, 2012).

The Neogene IBM volcanic front is spatially restricted to a few volcanic centers that are characterized by bimodal basaltic-andesitic and dacitic-rhyolitic eruptions. North of 31°N, six pairs of volcanic centers are identified with a uniform ~74 km spacing between them (Taylor, 1992). The volcanic front and the backarc rift both migrated northward at variable rates during the Neogene, during which time the extent and scale of explosive volcanism waxed and waned (Stern et al., 2003; Yamazaki & Stern, 1997).

### 4. IBM Expedition 352 Forearc Sediments

Shipboard investigations during IODP Expedition 352 (Reagan et al., 2015) indicate that the Oligocene-Recent sediments were deposited in extensional fault-controlled basins at three sites (Sites U1439-U1441), whereas condensed sedimentation, affected by current reworking, accumulated on a nearby fault-controlled basement high (Site U1442) (Figure 2). Two of the sites (Sites U1439 and U1442) were drilled on the upper forearc slope at a water depth of ~3150 m and the other two (Sites U1440 and U1441) on the lower forearc slope at ~4800 m. One to five lithological units are defined at each site depending on the recovery and lithological variability (Figure 2) (Reagan et al., 2015).



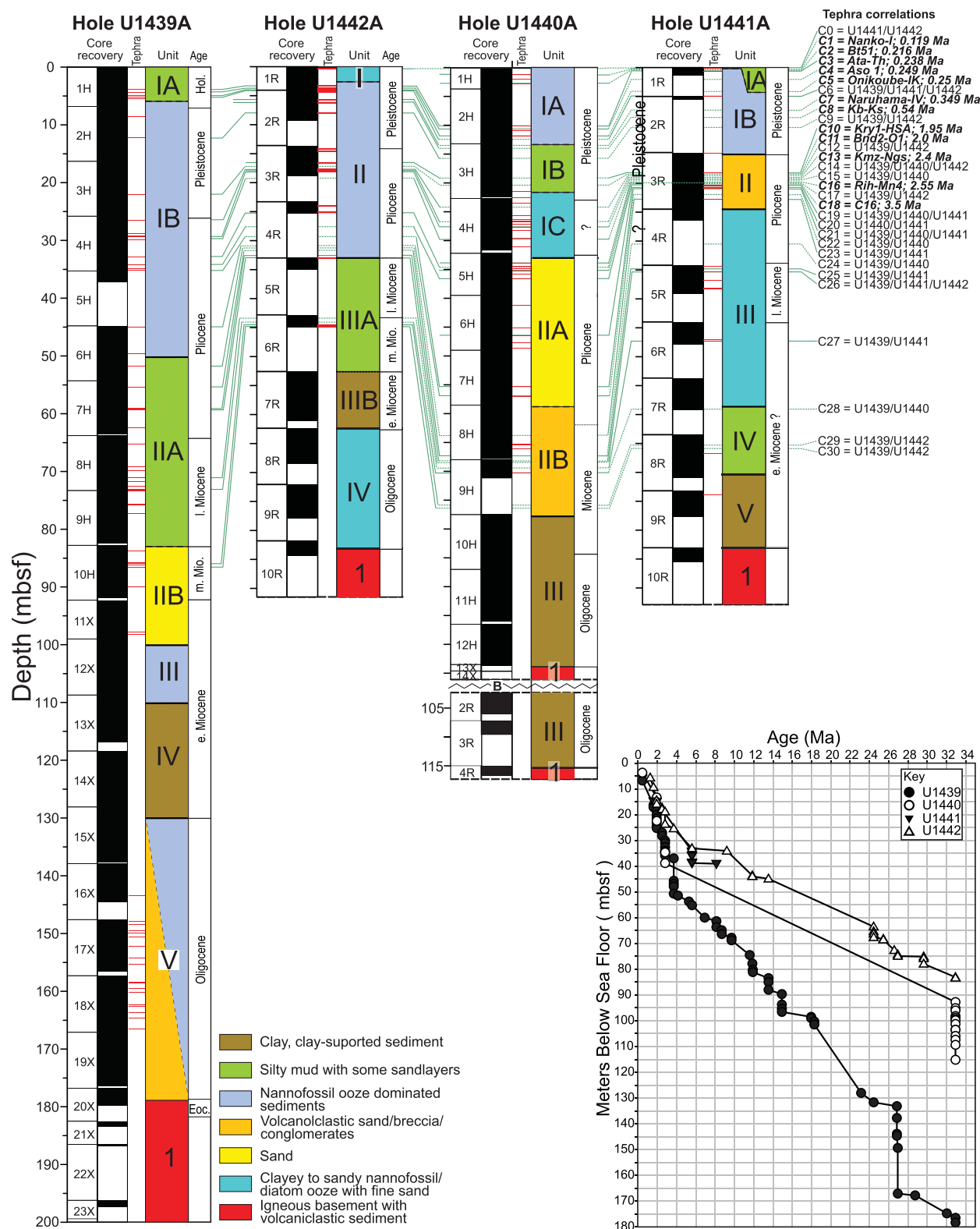


**Figure 2.** Lithostratigraphic columns for Sites U1439, U1440, U1441, and U1442 (from Reagan et al., 2015) with compositionally correlated ash layers CIB0 through CIB30 providing stratigraphic ties between the four sites of IODP Expedition 352. Correlations with known Japanese tephras (bold labels, solid purple lines) as discussed in the text and also the resulting age constraints for the Expedition 352 sediments are indicated to the right. Inset shows the age models for each site that are used to calculate the tephra ages (modified after Robertson et al., 2017). See Robertson et al., (2017) for further information concerning the biostratigraphy and the key zonal taxa that are used to construct the age models.

The oldest drilled sediments are characterized by Oligocene pelagic carbonates, accompanied by abundant tuffaceous sediments that accumulated in response to both gravity-controlled and air-fall processes (Reagan et al., 2015; Robertson et al., 2017). Early Miocene time was characterized by radiolarian-bearing mud and silty clay with hydrogenous metal-oxide precipitation with minimal tuffaceous input (Reagan et al., 2015; Robertson et al., 2017). Subsequently, during the Middle Miocene to Early Pliocene, pinkish nannofossil-bearing silty clays accumulated together with pinkish nannofossil ooze and minor amounts of air-fall tephra (Reagan et al., 2015; Robertson et al., 2017). During Early Pliocene to Recent sedimentation was characterized by weakly calcareous clay/claystone/mudstone, and nannofossil ooze with abundant air-fall tephra (Reagan et al., 2015; Robertson et al., 2017).

## 5. Methods

### 5.1. Sampling, Reworking, and Preparation

Expedition 352 drilled four sites in the IBM forearc (Sites U1439, U1440, U1441, and U1442) (Figure 1). Detailed description of drilling operations, recovery, laboratory methods, and core description are given in Reagan et al. (2015), including smear-slide observations of tephra. On this basis, 249 marine ash samples were initially selected for shore-based analysis. As an initial step it was necessary to separate primary fallout ash horizons from reworked ash. This was achieved using a combination of the shipboard data and post-cruise assessment of chemical composition. Heterogeneous glass compositions that do not show a clear magmatic differentiation trend were classed as reworked and excluded from the data set. However, some layers are more difficult to interpret. First, some of them show clear evidence of flow processes (e.g., graded bedding, parallel lamination). These layers are interpreted as the result of local reworking of primary fallout ash and so were included in the database. Second, some ash occurs as discontinuous subparallel remnants, termed ash pods, within the background hemipelagic sediments. Based on shipboard visual inspection, some of the ash pods were interpreted as primary tephra fallout that later underwent reworking or bioturbation (Reagan et al. (2015). Those ash pods that have homogenous glass compositions are confirmed as primary eruptive layers and are therefore included in the data base (indicated as pod layers in supporting information Table S1). Applying this approach 157 out of 249 samples have been identified as primary ash horizons.

For analytical treatment, ash samples were wet-sieved into different grain size fractions (63–125  $\mu\text{m}$ , 125–250  $\mu\text{m}$ , >250  $\mu\text{m}$ , and where necessary 32–63  $\mu\text{m}$ ). The 63–125  $\mu\text{m}$  fraction of the samples was embedded using epoxy resin into 12 predrilled holes on acrylic tablets and polished to facilitate measurements with electron microprobe (EMP) and a Laser Ablation Inductively Coupled Plasma Mass Spectrometer (LA-ICP-MS). All of the resulting major and trace element data and their respective errors are listed in supporting information Tables S1–S3.

### 5.2. Chemical Analysis

#### 5.2.1. Electron Microprobe (EMP)

Glass shards (~2,700 in total) were analyzed for major and minor elements on 189 epoxy embedded samples using a JEOL JXA 8200 wavelength dispersive EMP at GEOMAR, Kiel, utilizing the methods of Kutterolf et al. (2011). A calibrated measuring program was used based on international standards. Accuracy was monitored by standard measurements on Lipari obsidian (Lipari rhyolite; Hunt & Hill, 2001) and Smithsonian basaltic standard VGA. Sixty individual glass shard measurements were bracketed by two standard measurements per standard. Standard deviations of measured elements are <0.5% for major and <10% for minor elements (with the exception of  $\text{P}_2\text{O}_5$  and  $\text{MnO}_2$  in samples >65 wt.%  $\text{SiO}_2$ ). All of the analyses were normalized to 100% in order to eliminate the effects of variable postdepositional hydration and minor deviations in focusing of the electron beam. Analyses with total oxides <90 wt.% were excluded from the data set to avoid the effects of alteration that can affect all of the elements. Around 2,500 microprobe analyses finally passed the quality checks, which also excluded accidental shots on microcrystals. The acceptable analyses of each sample were then averaged in order to characterize the elemental compositions of each individual tephra.

#### 5.2.2. Laser Ablation-Inductively Coupled-Mass Spectrometry (LA-ICP-MS)

The trace element concentrations of ~300 glass shards (106 samples) were determined by LA-ICP-MS during February 2016 at the Academia Sinica in Taipei, Taiwan. The LA-ICP-MS instrumentation comprises a

laser beam (193 nm excimer laser) set to a spot size of 16–30  $\mu\text{m}$  (using 5–10  $\text{J}/\text{cm}^2$  energy density at 4–10 Hz repetition rate), coupled to a high-resolution ICP-MS. Following 45 s of blank acquisition, typical ablation times were around 75 s. Data reduction was performed using Version 4.0 of “real-time on-line” GLITTER© software (van Achterberg et al., 2001), immediately following each ablation analysis. Silica and calcium concentrations, measured by EMP, were used as an internal standard to calibrate the trace element analyses. An international glass standard (BCR-2g) was measured every five to eight samples in order to monitor accuracy and to correct for matrix effects and signal drift in the ICP-MS, and also for differences in the ablation efficiency between sample and reference material (Günther et al., 1999). The concentrations of NIST SRM 612, needed for external calibration, were taken from Norman et al. (1996). The limit of detection (LOD) for most trace elements was generally <100 ppb. For REEs, the LOD is generally around 10 ppb. The analytical precision is generally better than 10% for most trace elements.

### 5.3. Correlation Techniques

Ash-layer correlations are mostly based on chemical glass compositions, supplemented by modal compositions (e.g., crystals, lithic fragments, biogenic matter), sedimentary structures, textures of the pyroclasts, and stratigraphic relationships. Supporting data include the shape, vesicularity, and vesicle texture of glass shards and pumiceous fragments, and also the mineral content of the ash layers as determined in smear slides, both onboard (Reagan et al., 2015) and postcruise.

For each of the ash layers identified, 15 EMP analyses and 2–5 LA-ICP-MS analyses of individual glass shards were carried out on each sample. Individual ash layers were correlated with eruptive events within the Japan arc utilizing the tephra compositions of Kimura et al. (2015) and references therein. The onshore-offshore correlations were achieved by comparing the average composition of each analyzed marine ash bed with documented terrestrial ash beds. Ash beds are defined as being correlative when their compositions overlap, within the error for each sample and for each element analyzed (gray bars in diagrams). The correlations are thereby constrained by multiple geochemical overlaps of major elements and, where appropriate, also trace elements (see Figures 6, 8, and 10). In addition to analytical errors, possible correlations are limited by alteration effects, especially for the older (i.e., Neogene) marine and terrestrial data in which diagenesis may have altered some but not all of the element concentrations. Accordingly, we utilize element ratios that effectively minimize the influences of both analytical errors and alteration.

Ash beds that can be correlated across different sites and/or with tephra on land are defined as a “tephra layer” (CIB0 – 30; CIB for correlation “Izu-Bonin”). Thus, a “tephra layer” that represents a single volcanic eruption may include multiple “ash beds/layers” that occur in several drill holes at one or more sites. The numeric order of the “tephra layer” increases with age.

## 6. Tephrochronology

### 6.1. Age Models From Biostratigraphy

The biostratigraphic component of the age model was constructed primarily using calcareous nannofossil assemblages, with additional age constraints from radiolarian assemblages, as reported elsewhere (Robertson et al., 2017). Calcareous nannofossils were identified in smear slides that were made using standard techniques (Reagan et al., 2015). The samples were examined using a light microscope with an oil immersion lens in both plane-polarized and cross-polarized light at 1,000X magnification. The standard nannofossil zonations by Martini (1971), Bukry (1973, 1975), and Okada and Bukry (1980) were utilized in order to evaluate nannofossil age datums. The website Nannotax ([www.nannotax.org/](http://www.nannotax.org/)) was consulted for updated nannofossil genera and species ranges. The zonal scheme of Martini (1971) was selected for the biozones, and this zonal scheme was correlated with the geological timescale of Gradstein et al. (2012).

Where calcareous nannofossils are rare or absent, additional samples were taken for radiolarian biostratigraphy. Radiolarian-bearing samples were processed following the method outlined in De Wever et al. (2001). Once processed, sieved residues were transferred to crucibles and dried in an oven at 60°C. The residues were viewed under a binocular microscope and well-preserved radiolarian tests were transferred to a SEM stub and mounted on carbon tape. Stubs were placed in a SEM at the University of New England, Armidale, and photomicrographs were taken of the tests. These images were compared to published photographs of known species and the age and distribution of these species were used to determine an assemblage age

**Table 1**

Summary of Ash Layer Correlations WITHIN the Expedition 352 Sediments and Also With Japanese and Izu-Bonin Sources, Including Calculated Tephra Volumes and Eruption Magnitudes

CIB # <sup>a</sup>	Ash layers	Age (Ma) from sedimentation rates and correlations	Correlations to well-dated Japanese tephras/Japanese source regions	Correlations to IBM source regions <sup>c</sup>	Estimated tephra volumes (km <sup>3</sup> ) <sup>d</sup>	Estimated eruption magnitudes <sup>e</sup>	Representative elements and concentrations for IBM/Japan differentiation					
							K <sub>2</sub> O	SiO <sub>2</sub>	CaO	Th/La	Rb/Hf	Zr/Nb
<b>C0</b>	U1441A-1R-1_22–24 average	0.029	-	<b>II</b>	27	6.7	0.91	63.48	10.93	0.108	5.69	72.87
	U1442A-1R-1_55–57 average	0.034					0.87	63.28	10.78	-	-	-
<b>C1</b>	U1440A-1H-1_139–141 average	0.119	<b>Nanko-I; 0.119 Ma; SW Japan</b>	-	<b>90</b>	<b>7.2</b>	2.06	71.17	22.61	0.386	16.53	24.41
<b>C2</b>	U1440A-1H-2_89–91 average II	0.216	<b>BT51; 0.216 Ma; NE Japan</b>	-	<b>16</b>	<b>6.4</b>	2.66	77.33	60.17	-	-	-
<b>C3</b>	U1439A-1H-3_97–99 average	0.223	<b>Ata-Th; 0.238 Ma; Kyushu</b>	-	<b>306 (1950)<sup>b</sup></b>	<b>7.7 (8.5)<sup>b</sup></b>	2.99	78.47	66.23	0.462	34.22	12.37
	U1440A-2H-4/5_144–67 average	0.238					3.52	77.88	77.13	0.483	42.08	10.99
	U1441A-1R-1_76–78 average	0.238					2.92	78.03	62.33	0.449	39.58	11.04
	U1442A-1R-3_97–99 average II	0.238					2.81	78.08	57.37	-	-	-
	U1442A-1R-4_11–13 average I	0.270					2.95	78.24	62.90	-	-	-
<b>C4</b>	U1439A-1H-3_143–145 average	0.249	<b>Aso1; 0.249 Ma; Kyushu</b>	-	<b>140</b>	<b>7.4</b>	5.21	67.94	37.76	0.351	22.83	19.77
	U1442A-1R-4_11–13 average 2	0.270					5.17	67.92	34.03	-	-	-
<b>C5</b>	U1439A-1H-4_53–55 average	0.298	<b>Onikoube-IK; 0.25 Ma; NE Japan</b>	-	<b>345</b>	<b>7.7</b>	1.72	76.41	41.09	0.388	10.15	42.42
	U1440A-2H-6_95–97 average	0.250					1.47	77.45	40.32	0.346	13.91	34.72
	U1442A-1R-4_87–89 average	0.308					1.69	76.28	40.82	-	-	-
<b>C6</b>	U1439A1H-4W-77–79 average	0.319	<b>- / Kyushu</b>	-	9	6.1	1.36	58.02	8.23	-	-	-
	U1441A-2R-1_6–8 average	0.312					1.50	60.72	10.26	0.381	39.17	7.51
	U1442A-1R-4_101–103 average 1	0.315					1.41	59.40	9.15	-	-	-
<b>C7</b>	U1442A-2R-1_36–38 average	0.349	<b>Naruohama-IV; 0.349 Ma; Kyushu</b>	-	<b>35</b>	<b>6.7</b>	2.69	78.32	58.04	0.413	15.47	31.53
<b>C8</b>	U1442A-2R-2_14–16 average	0.540	<b>Kb-Ks; 0.54 Ma; Kyushu</b>	-	<b>49</b>	<b>6.9</b>	4.21	74.72	62.67	0.539	30.18	20.84
<b>C9</b>	U1439A-2H-4_100–102 average	1.117	<b>- / Kyushu</b>	-	-	-	3.10	74.83	39.86	0.455	24.06	20.06
	U1442A-2R-3_102–104 average	1.050					3.24	75.83	45.04	0.379	26.68	16.40
<b>C10</b>	U1441A-3R-3_60–62 average	1.950	<b>Kry1-HSA; 1.95 Ma; Kyushu</b>	-	<b>47</b>	<b>6.8</b>	1.73	78.52	48.88	0.118	5.18	35.27
	U1442A-3R-3_0–2 average	1.950					1.42	77.41	45.60	0.195	6.31	37.28
<b>C11</b>	U1439A-3H-4_134–136 average	2.167	<b>Bnd2-O1; 2.0 Ma; C-Japan</b>	-	<b>60</b>	<b>6.9</b>	3.26	75.90	50.88	0.432	26.86	16.43
<b>C12</b>	U1439A-4H-1_75–77 average	2.460	<b>- / C-Japan</b>	-	-	-	3.57	77.53	71.23	0.526	51.90	9.60
	U1442A-3R-3_121–123 average	2.297					3.61	77.61	69.62	0.361	53.80	7.39
<b>C13</b>	U1442A-3R-4_7–9 average	2.400	<b>Kmz-Ngs; 2.4 Ma; Kyushu</b>	-	<b>47</b>	<b>6.8</b>	2.87	75.13	48.67	-	-	-
<b>C14</b>	U1439A-4H-3_65–67 average	2.735	<b>- / Kyushu</b>	-	50	6.9	3.01	78.07	56.57	0.534	26.08	24.66
	U1440A-4H-4_57–59 average	2.216					3.33	77.32	63.43	0.496	19.71	25.33
	U1442A-3R-4_9–11 average	2.402					3.02	77.72	55.78	-	-	-
<b>C15</b>	U1439A-4H-3_92–94 average	2.763	-	<b>I</b>	3	5.5	0.86	70.65	18.19	0.120	5.30	84.42
	U1440A-4H-6_1–3 average	2.346					0.99	70.63	19.54	-	-	-
<b>C16</b>	U1440A-5H-2_34–36 average II	2.550	<b>Rih-Mn4; 2.55 Ma; C-Japan</b>	-	<b>42</b>	<b>6.8</b>	1.71	75.63	37.87	0.296	5.68	48.40
<b>C17</b>	U1439A-4H-6_5–7 average	3.169	<b>- / C-Japan</b>	-	28	6.6	3.13	78.05	81.31	0.454	37.99	11.69
	U1442A-4R-CC_2–4 average	3.169					4.33	77.70	172.77	0.499	39.03	7.18
<b>C18</b>	U1440A-5H-3_9–11 average	3.500	<b>C16; 3.5 Ma; NE Japan</b>	-	<b>150</b>	<b>7.3</b>	3.04	78.45	82.06	0.467	20.29	25.53
<b>C19</b>	U1439A-4H-7_7–12 average	3.348	-	<b>III</b>	24	6.5	0.26	54.73	5.92	0.075	3.37	91.11
	U1440A-5H-3/4_148–6 average	3.529					0.31	56.62	6.65	0.089	3.49	109.09
	U1441A-3R-4_134–136 average	3.348					0.34	57.19	7.17	0.100	5.13	40.73
<b>C20</b>	U1440A-6H-5W-106–108 average	3.728	-	<b>IV</b>	64	7.0	0.57	72.70	20.73	-	-	-
	U1441A-3R-5_20–22 average	3.429					0.66	72.90	20.45	0.103	6.42	66.03
<b>C21</b>	U1439A-4H-CC_21–23 average	3.477	-	<b>III</b>	6	5.9	0.31	54.46	5.51	-	-	-
	U1440A-7H-5_54–56 average	3.907					0.33	54.71	5.50	0.127	3.61	114.11
	U1441A-3R-5_41–43 average	3.477					0.33	54.65	5.53	0.111	3.66	112.08
<b>C22</b>	U1439A-6H-1_25–27 average	3.941	-	<b>III</b>	6	5.9	0.59	73.15	21.28	0.080	5.71	67.47
	U1440A-7H-6_70–72 average	3.941					0.60	72.16	18.73	0.122	4.19	97.76
<b>C23</b>	U1439A-6H-6W-6–8 average	4.309	-	<b>III</b>	10	6.2	0.89	57.20	7.59	-	-	-
	U1441A-3R-6_76–78 average	4.309					0.39	57.67	7.05	0.122	4.04	85.34
<b>C24</b>	U1439A-7H-1_117–119 average II	5.717	<b>- / SW Japan</b>	-	50	6.9	1.60	66.89	16.94	0.224	7.97	21.45
	U1440A-8H-6_51–53 average I	8.735					1.49	67.65	17.90	-	-	-
<b>C25</b>	U1439A-7H-4_36–45 average	7.259	-	<b>II</b>	30	6.7	0.37	56.33	6.22	0.131	4.48	104.61
	U1441A-5R-1_39–41 average	7.259					0.38	56.31	6.33	0.110	3.80	106.37
<b>C26</b>	U1439A-7H-4_61–63 average	7.333	-	<b>II</b>	10	6.2	0.34	55.58	6.04	0.083	4.26	119.05
	U1441A-5R-1_128–130 average	7.330					0.36	56.47	6.40	0.115	5.36	120.14
	U1442A-5R-1_7–9 average	7.330					0.32	57.34	6.83	0.109	3.64	93.24
<b>C27</b>	U1439A-8H-5_147–149 average	10.419	-	<b>II</b>	17	6.4	0.99	76.02	30.85	0.084	7.52	86.85
	U1441A-6R-3_52–54 average	10.419					0.80	76.26	30.13	-	-	-
<b>C28</b>	U1439A-8H-CC_1–3 average	10.862	-	<b>IV</b>	18	6.4	0.51	71.04	17.95	-	-	-
	U1440A-9H-1_80–82 average	10.419					0.56	70.43	16.68	0.088	3.85	149.79
<b>C29</b>	U1439A-10H-3_48–50 average	14.168	<b>- / NEJapan</b>	-	40	6.8	4.99	76.61	94.24	0.278	18.62	12.52
	U1442A-6R-2_88–90 average	14.239					4.84	76.16	100.37	0.362	15.59	15.58
<b>C30</b>	U1439A-10H-3_88–90 average	14.257	-	<b>II</b>	7	6.1	1.08	76.14	26.67	0.164	5.92	102.29
	U1442A-6R-CC_1–3/4–6 average	14.257					0.80	76.28	26.98	0.117	4.21	103.46

<sup>a</sup>Correlations between sites.

<sup>b</sup>Eruptive values for extended thickness of 83 cm.

<sup>c</sup>I = S-IBM; II = C-IBM-reararc; III = C-IBM-arc; IV = N-IBM.

<sup>d</sup>Averages per individual Japanese eruptions and averaged for proposed IBM and Japanese source regions.

<sup>e</sup>Magnitudes per individual Japanese eruptions and averaged for proposed IBM and Japanese source regions.



for each sample (see Robertson et al., 2017). The biozones of Kamikuri et al. (2009) were used as the primary reference for this study.

## 6.2. Tephra Ages

Biostratigraphic datums provide age constraints for the drilled sediments (see methods). Additionally, as shown below, 22 marine ash beds in several of the Expedition 352 sites can be geochemically correlated with 12 specific deposits that resulted from eruptions of known ages in Japan within the last 3.5 Ma. These tephra layers provide additional time lines that can be used to optimize age models based on micropaleontology.

Using the combined timelines, the intervening thicknesses of marine sediments were converted to (hemi-) pelagic sedimentation rates (see also Robertson et al., 2017). The sedimentation rates inferred between two “age anchors” are necessarily averages resulting from linear interpolation. The calculated sedimentation rates allow estimates of the ages of the other tephra layers, assuming that sedimentation rates remained constant within the intervening time intervals. The ages obtained from the calculated sedimentation rates provide additional support for ash correlations in cases where geochemical correlations are uncertain.

The tephra ages can have errors of up to 14% of their calculated age, which result from uncertainties in the determination of sedimentation rate (cf., Kutterolf et al., 2013). Compaction and drilling disturbance especially in the deeper parts of the holes may cause differences in age determinations as a result of overestimation or underestimation of sedimentation rates. Another source of error is the thickness of the ash beds, which may obscure the true background sedimentation rate due to near-instantaneous emplacement (Kutterolf et al., 2008c). A further, although minor, potential source of error is variable admixing of volcanic ash particles in some background intervals, which would lower calculated ages. Such limitations are discounted here because the cumulative thickness of the ash beds amounts to only ~0.7% (U1442) to ~2.8% (U1440) of the total sediment thickness, with an average of 1.7% for all of the recovered sediments.

Overall sedimentation rates of 2–62 m/Ma on the upper slope (Sites U1439/U1442) and 1–360 m/Ma on the lower slope (Sites U1440/U1441) are inferred, although the apparent sedimentation rates may vary with depth (Robertson et al., 2017). The ages estimated for the ash layers encompass the Late Eocene–Early Oligocene to latest Pleistocene. The youngest recovered ash bed has an estimated age of ~30 ka at Sites U1441 and U1442, whereas the oldest ash bed at Site U1439 is estimated to have an age of 32.3 Ma (Table 1 supporting information Table S1).

## 7. Tephra Inventory

Below shipboard observations (e.g., core description, shipboard petrography; Reagan et al., 2015) are combined with the new data from the analytical methods, complemented by reassessment of core pictures and smear slides to provide a comprehensive tephra inventory for the Expedition 352 sediments.

Of 157 identified distinct ash layers, horizons of ash pods (i.e., discontinuous layers or inclusions), and dispersed intervals of ash ranging from 0.5 to 41 cm in thickness (Figure 3) (Reagan et al., 2015), 102 (64%) are light gray to white (pink) felsic ashes, 27 (17%) are gray layers suggesting an intermediate composition, and 28 (18%) are black layers of mafic composition.

In general, the ash layers are massive and have a sharp basal contact with the underlying marine sediments, which is most obvious in sediments drilled with the APC (advanced piston coring) system. These ash layers are commonly well sorted to very well sorted, show normal grading in grain size and also a several-centimeter-thick transition to the overlying sediment (Figure 3). A minority of the ash beds show moderate to poor sorting, variably developed cross-lamination or convolute bedding, basal erosional features, and also density grading of minerals and juvenile clasts, especially in the Oligocene section of Site U1439.

The average grain size within individual ash layers ranges from coarse silt to medium sand (i.e., 32–500  $\mu\text{m}$ ). The ash beds are generally nonbioturbated or weakly bioturbated in contrast to the interbedded sediments. Some ash layers are significantly indurated compared to their host sediment as a consequence of diagenetic processes. Unconformable and/or inclined bedding of ash beds, caused by drilling disturbance, erosion, creep, slumping, or tectonic tilting are locally present, especially at Sites U1441 and U1442. However,

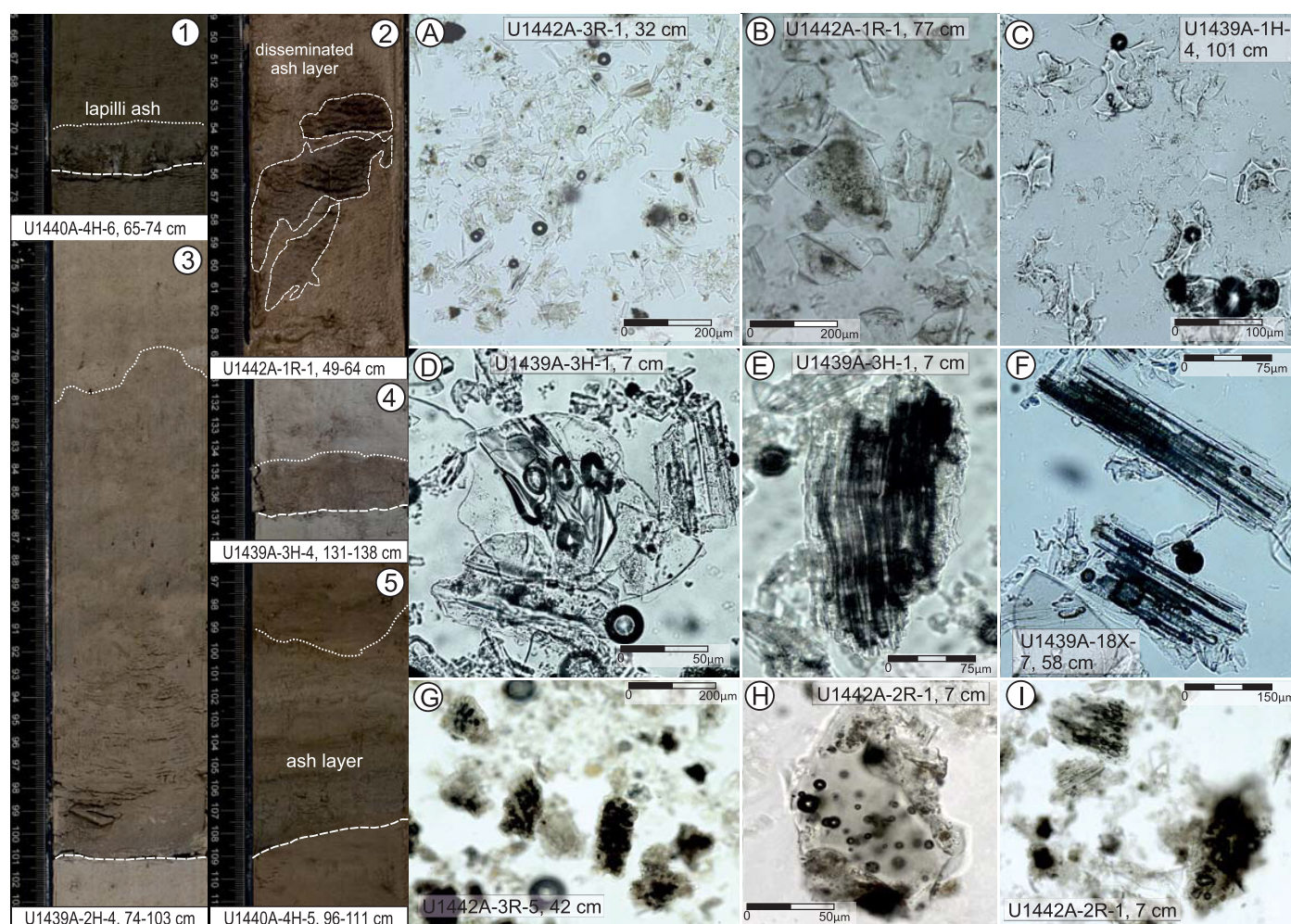


**Figure 3.** Photographs of selected felsic ash layers (1–5) and microphotographs of smear slides showing glass shard textures of (a–f) silicic and (g–i) mafic ash layers. (a) and (b) Dense blocky glass shards; (c) cusped glass shards formed by fragmentation of “foamy” pyroclasts with predominantly large, rounded, or elliptical bubbles; (d) Rounded and elliptical vesicles within blocky and cusped glass shards; (e) and (f) pumiceous clast with tubular vesicles; (g) pumiceous brownish clasts with clusters of elongate and elliptical vesicles; (h) and (i) Dense brownish glass shards with some round and elliptical vesicles.

such features were also largely obscured by RCB (rotary core barrel) drilling of the sediment column at these two sites (Figure 3). Some ash layers are disseminated throughout adjacent sediment by drilling or “in situ” reworking (Figure 3). Within these intervals, the dispersed glass shards have homogenous compositions and textures suggesting that they can be correlated with primary eruptive events.

The felsic ash layers are dominated by transparent volcanic glass with rare but persistent occurrences of plagioclase, and variable occurrences of quartz, amphibole, clinopyroxene, orthopyroxene, and traces of biotite. The mafic ash layers contain (light-)brown and red-brown glass—if tachylitic (microcrystalline) dark pyroclasts—together with common feldspar and trace amounts of pyroxene and olivine. The mineral contents of the ash beds range from mineral-poor (1–5 vol.%) to mineral-rich (up to 50 vol.%). Crystal-rich intervals particularly occur at the base of some coarse ash beds indicating the presence of normal density grading.

The relative abundances of glass shard colors, textures, and vesicles define six overall tephra texture groups that are recognized at the different marine sites: (1) colorless glass shards that are characterized by predominant dense, blocky, and commonly cusped shards together with common tubular vesicular pumiceous clasts; (2) transparent, highly vesicular pyroclasts exhibiting predominantly pumiceous and fibrous clasts with tubular-shaped vesicles, and common dense and cusped glass shards with elongated vesicles; (3) a transitional group with colorless to light brownish pyroclasts of tubular and elongate vesicle-rich pumiceous

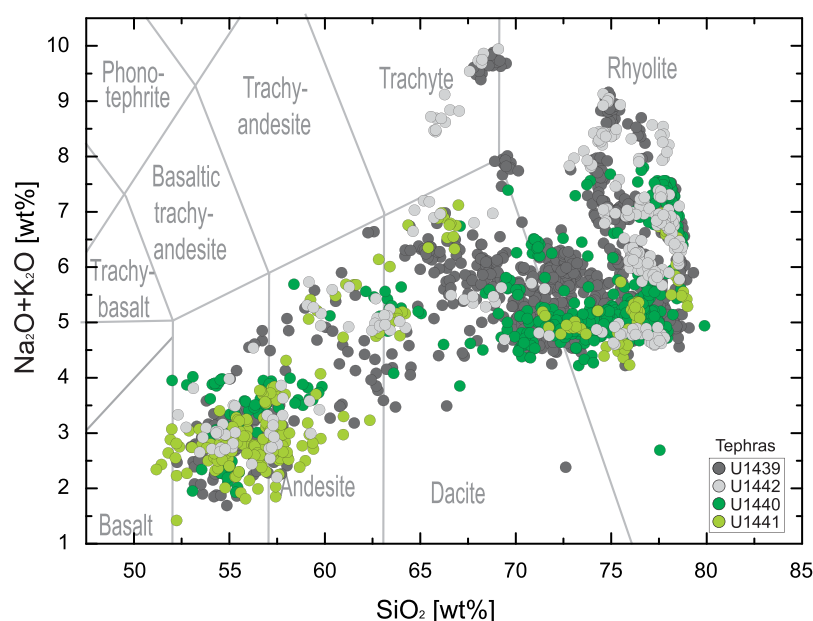


**Figure 4.** Total alkali versus silica plot showing the compositional variability in Expedition 352 tephra and discrimination of volcanic rock classes (after Le Maitre et al., 2002). All data are normalized to anhydrous compositions.

clasts together with less abundant cusped and blocky-shaped, predominantly dense glass shards; (4) a mostly light brown pyroclast group made up of a mixture of abundant cusped and blocky, predominantly dense glass shards together with less abundant highly vesicular, tubular pumiceous grains; (5) mostly crystal-rich ash layers with nearly equal mixtures of brown or colorless pumiceous, blocky, and cusped pyroclasts having a bimodal distribution of the predominant vesicle types with numerous rounded and elliptical forms together with abundant tubular vesicles; and (6) dark gray to black ash containing a mixture of predominantly blocky, brownish, mafic glass shards of moderate vesicularity and mostly rounded and elliptical gas bubbles (Figure 3).

Taken as a whole, the analyzed glass shards of 136 ash layers encompass basaltic andesitic to rhyolitic compositions (Figure 4) with rare trachytic exceptions. Additionally, eight of the ash beds show mixing between dacite and rhyolite, two between basalt and dacite; there are also 11 ash horizons where bimodal compositions can be observed. Comparing the individual drill sites, three of these (Sites U1439, U1440, U1442) contain between 75% and 85% of ash layers with  $\text{SiO}_2 > 65\text{wt.}\%$ , consistent with the general trend described above. In contrast, Site U1441 encompasses an exceptionally large number of ash layers (68.4%) in the tephra inventory with  $<65\text{ wt.}\% \text{ SiO}_2$ , confirming the shipboard smear slide observations (Figure 5).

From the texture and appearance of all of the ash layers and combined with their chemical homogeneity, we infer that they all represent primary volcanic events. The ash beds were dominantly emplaced by air-fall (e.g., well-sorted, normal graded). In addition, a small number of the ash layers, of exclusively Oligocene age, are interpreted as having accumulated from pyroclastic density currents (e.g., cross-laminated, poorly sorted examples). These deposits are characterized by cross lamination and in the uppermost part by concentrations of fine, rounded, relatively low-density pumice lapilli, whereas

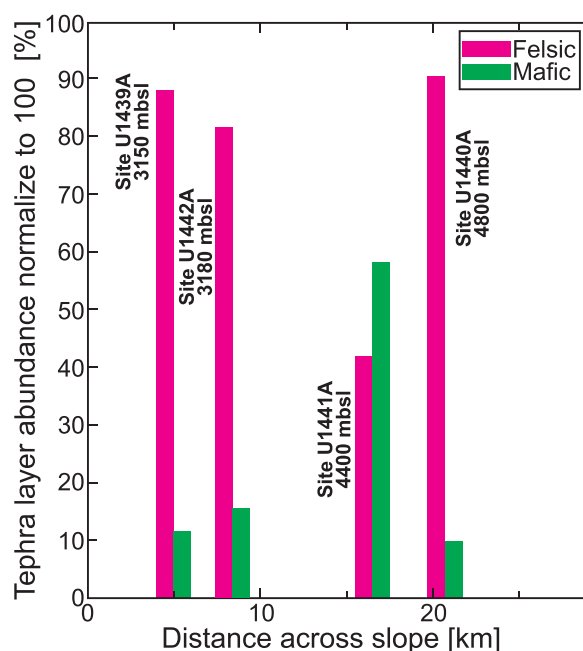


**Figure 5.** Normalized ash abundance for Sites U1439–U1442, modified after Reagan et al. (2015). Marine tephra are grouped into mafic and felsic types on the basis of compositional glass data and a threshold of 60 wt.% silica to distinguish between felsic and mafic tephra. Note the different amounts of felsic and mafic ash layers across the IBM forearc slope. Depths are shown in meters below sea level (mbsl).



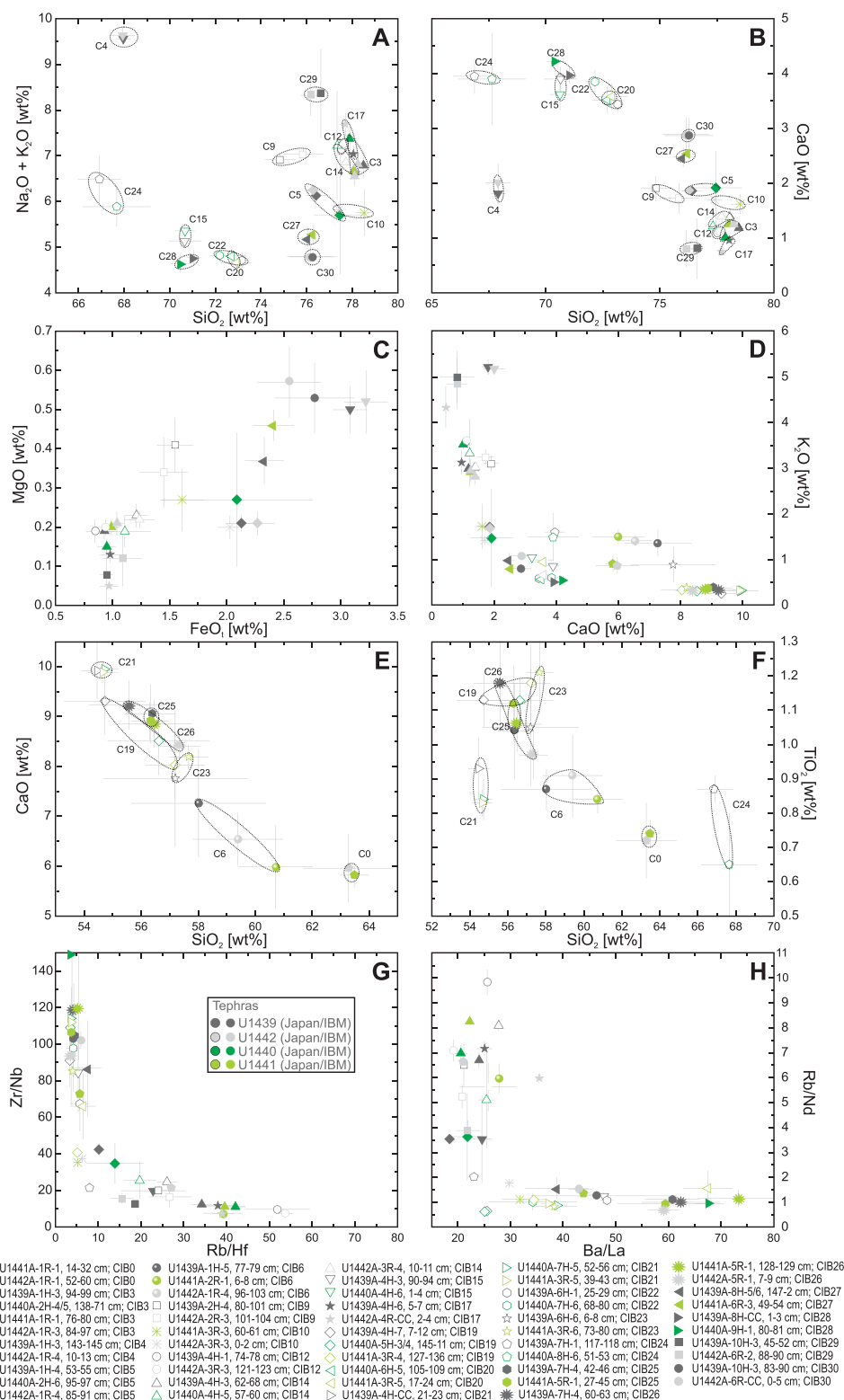


**Figure 6. (a–h) Major and trace element glass shard compositions of Expedition 352 tephras illustrating site-to-site correlations.** Dashed circles in Figures 6a, 6b, 6e, and 6f show examples of site-to-site correlations. The number “Cx” is used to refer to the respective CIB correlation number given in the text and the supporting information (Tables S1–S3). The data represent averages of 10–20 (EMP) or 2–7 (LA-ICPMS) single point measurements; the gray bars indicate the compositional range within each sample. All major element data are normalized to anhydrous compositions.



the base of the beds shows relatively dense mineral concentrations. The pyroclastic material erupted on land or beneath the sea and was then transported by gravity-flow processes (mostly turbidity currents) to their present position.

## 8. Correlations and Provenance

The geochemical compositions of all 157 identified ash layers recovered from four Expedition 352 sites can be used for regional correlation and provenance analysis.

Correlations can be established between the marine ash layers at the different sites, and also with possible parental terrestrial tephra deposits and source volcanoes. We use well-tested major and trace element variation diagrams that have been found by extensive application to be useful for chemical correlation using the Expedition 352 tephra inventory (e.g., (Bryant et al., 1999; Clift & Blusztajn, 1999; Kutterolf et al., 2008b, 2016; Lowe, 2011; Lowe et al., 2008; Pearce et al., 2007, 1999; Schindlbeck et al., 2016a; Westgate et al., 1994).

Reflecting the wide range of chemical compositions, separate “panels” were created to show the mafic and felsic compositions for major elements (i.e., major elements: total alkali,  $K_2O$ , or  $TiO_2$ , or  $CaO$ ,  $MgO$  versus  $SiO_2$ ,  $FeO_t$ , and  $CaO$ ; Figure 6a–6f). Trace elements and trace-element-ratio diagrams complement the major-element plots by further distinguishing tephra and establishing robust correlations (Figures 6g and 6h; e.g.,  $Zr/Nb$  versus  $Rb/Hf$ ,  $Rb/Nd$  versus  $Ba/La$ ). As a result, we are able to establish 31 marker tephra layers (CIB0 to CIB30), comprising 62 individual ash layers that correlate between the Expedition 352 drill sites and/or with known eruptions in Japan, as discussed below.

### 8.1. Ash-Layer Correlation Between Holes and Sites

For all four drill sites, we are able to establish 24 site-to-site correlations using the chemical discrimination diagrams (Figure 6) (see also supporting information Table S1). One tephra layer (CIB3) can be correlated between all four sites, six tephra layers (CIB 5, 6, 14, 18, 20, 25) between three sites, and seventeen tephra layers between two sites (CIB 0, 4, 9–10, 12, 15, 17, 19, 21–24, 26–30) (Table 1). The correlated tephra layers provide tie lines, and the time markers when correlated with onshore deposits (see below), that are necessary to generate a complete tephrochronostratigraphy across the sites.

### 8.2. Provenance and Correlations to Specific Eruptions From Japan

The analyzed marine ash layers can usefully be divided into an “island arc-like type” versus a “continental arc-like” type. The former has an IBM arc/backarc origin and the latter a Japan origin. This interpretation was achieved by comparing a series of ratios (e.g., Schindlbeck et al., 2018), namely  $SiO_2/CaO$ ,  $La/Sm$ ,  $Zr/Nb$ ,  $Th/Yb$ ,  $Ta/Yb$ ,  $Rb/Hf$ ,  $Ba/La$ ,  $U/La$ ,  $Ba/Th$ , and  $K_2O$  (Figure 7) with equivalent ratios available for IBM volcanic matter in the literature (e.g., Amma-Miyasaka & Nakagawa, 1998; Arculus & Bloomfield, 1992; Bryant et al., 2003; Fiske et al., 2001; Fujioka et al., 1992; Gill et al., 1994, 1992; Hamada & Fujii, 2007; Hochstaedter et al., 2001; Ishizuka et al., 2007, 2006; Nakano & Yamamoto, 1987; Rodolfo et al., 1992; Shukuno et al., 2006; Straub, 2003, 2017; Straub et al., 2009, 2010; Tamura et al., 2005, 2007, 2009; Tani et al., 2008; Taylor & Nesbitt, 1998; Togashi & Terashima, 1997; Tollstrup et al., 2010; Yuasa, 1995) and also Japanese volcanic rocks (e.g., Hirose et al., 2014; Ikehara, 2015; Kimura et al., 2010, 2015; Machida, 1999, 2002; Moriwaki et al., 2008; Nagahashi & Kataoka, 2014; Nagahashi et al., 2003, 2004; Nakano & Yamamoto, 1987; Satoguchi & Nagahashi, 2012). The analyzed ash layers at Sites U1439–U1442 can be divided into 101 ash layers that are likely to have originated from an oceanic arc-related source like IBM, and 56 of inferred continental arc provenance (high  $U/La$ ,  $Rb/Hf$ ,  $La/Sm$ ,  $Th/Yb$ ,  $K_2O$ ), probably from Japan. For the latter category, variable trace element ratios are grouped into clusters, which probably reflect subtly different Japanese arc provenances. Using the same literature data, further discrimination is possible between potential origins from North-East Japan (NEJ), Central Japan (CJ), South-West Japan (SWJ), and Kyushu (KY) (Figures 8a and 8b). We also take account of the provenance fields of major volcanic centers such as Aso Volcano on Kyushu, Ontake Volcano in Central Japan, and Daisen Volcano in South-West Japan. Most of the marine tephra assigned to a Japan origin show a clear overlap with the Kyushu and Central Japan provenance field (e.g., high  $Rb/Hf$  and  $La/Yb$ ), or with North East Japan provenance field (e.g., low  $Ba/Zr$ ,  $Rb/Hf$  and  $La/Yb$ ). A few tephra can also be assigned to a Southwest Japan provenance.

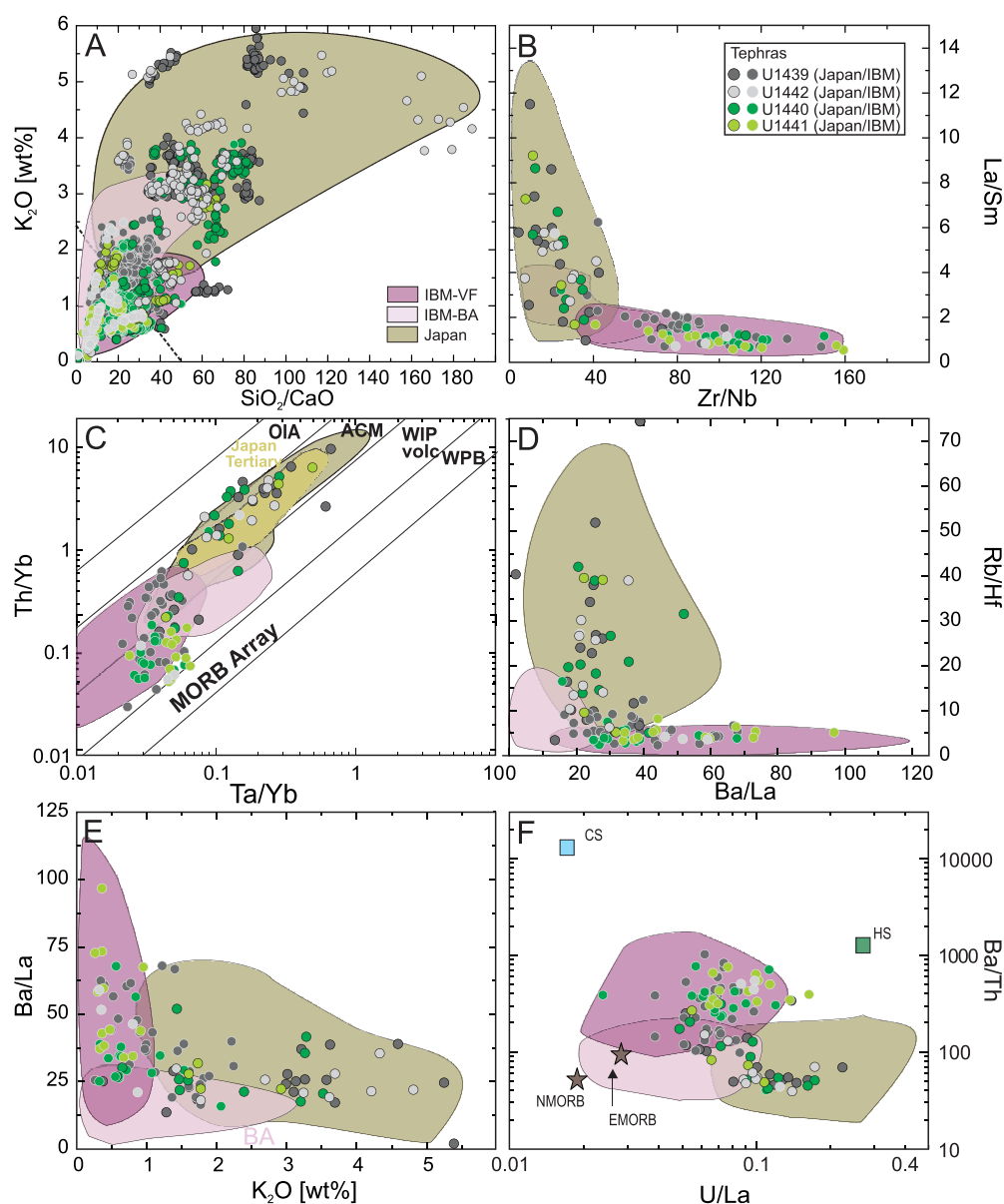


**Figure 7.** Marine tephra from Expedition 352 compared to regional compositional fields indicating a Japanese, IBM volcanic front, or IBM back arc provenance (see references in the text). (a)  $\text{SiO}_2/\text{CaO}$  versus  $\text{K}_2\text{O}$ , (b)  $\text{Zr/Nb}$  versus  $\text{La/Sm}$ , (c)  $\text{Th/Yb}$  versus  $\text{Ta/Yb}$  (modified after Gorton & Schandl, 2000), (d)  $\text{Ba/La}$  versus  $\text{Rb/Hf}$ , (e)  $\text{K}_2\text{O}$  versus  $\text{Ba/La}$ , (f)  $\text{U/La}$  versus  $\text{Ba/Th}$  (modified after Patino et al., 2000). OIA = ocean island arc; ACM = active continental margin; WIPvolc = within plate volcanics; WPB = within plate basalts; CS = carbonate sediment; HS = hemipelagic sediment. The data represent the averages of all of the analyses of each individual tephra.

Some of the marine ash layers of inferred Japan mainland provenance can be further assigned to specific eruptions using the database of Kimura et al. (2015) (utilizing the colored correlation fields). Correlations of major element compositions are shown in Figures 8c–8f. Where possible, we complement the data with additional average compositions from the literature (e.g., Ikehara, 2015; Machida, 1999, 2002; Moriawaki et al., 2008; Nagahashi et al., 2003; Satoguchi & Nagahashi, 2012). Twelve correlations (tephra layers CIB 1–5, 7–8, 10–11, 13, 16, and 18) can be established between the marine ash layers and the specific Japanese eruptions, ranging in age from 0.119 to 3.5 Ma (Figures 8c–8f; Table 1). As a result, at Site U1440, we can identify a marine equivalent of the Nankai-I and BT51 tephra that erupted 119 and 216 ka ago from an unknown source (correlation CIB1 and CIB2). Tephra layers CIB 3 and CIB 4 correlate with the well-known Ata-Th eruption (238 ka, Ata Caldera) and the potassium-rich Aso-1 (249 ka; Aso Caldera) eruption; these

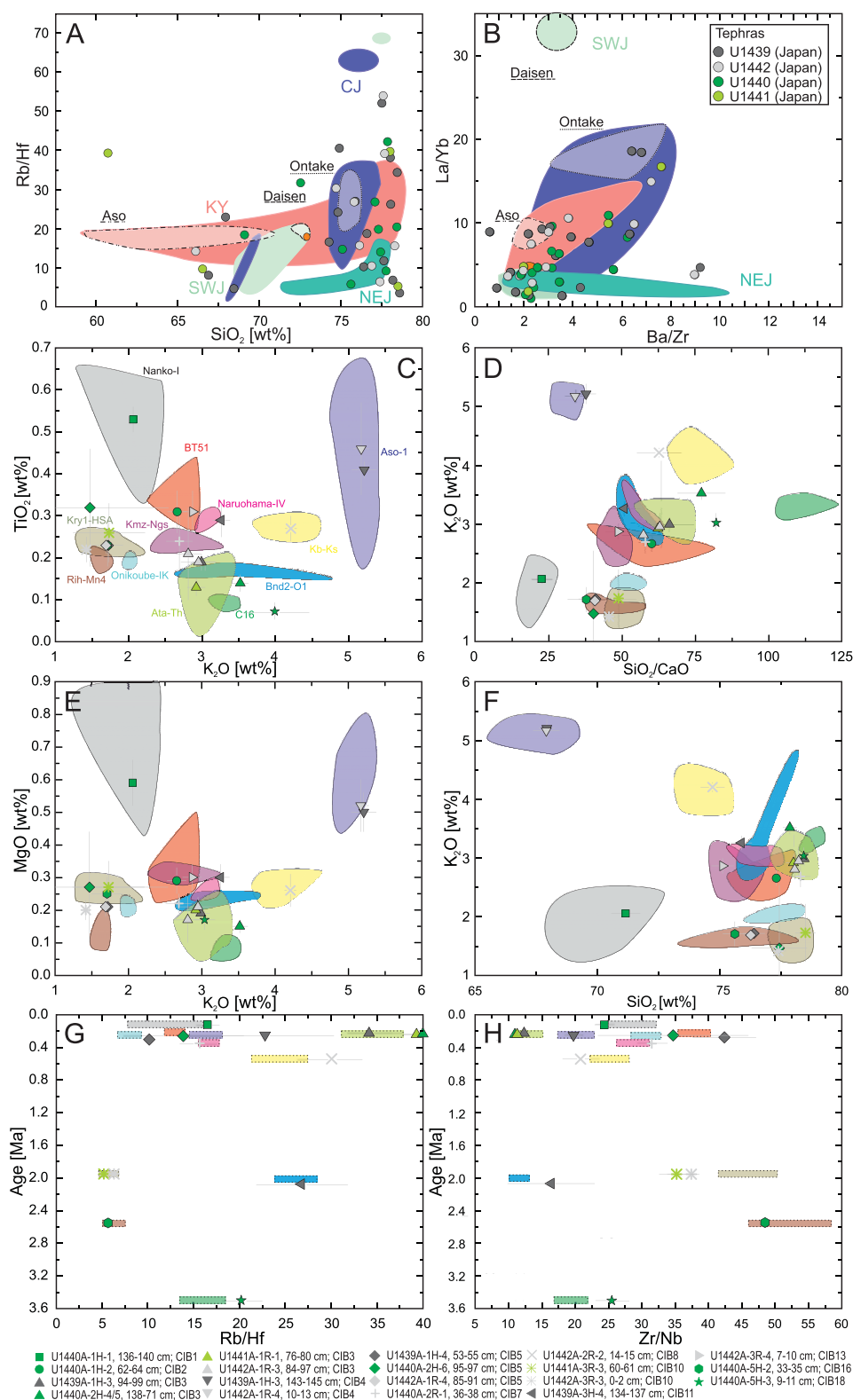


**Figure 8.** (a) through (f) Ash layers from Expedition 352 with a Japanese origin compared with the fields of proximal Japanese tephras as summarized in Kimura et al. (2015) and references therein (see main text), (g) Rb/Hf versus age, and (h) Zr/Nb versus age. Data are averages of all of the analyses made for each individual tephra horizon. Gray bars represent the compositional range of each sample; letters in the key and in the diagrams identify CIB-layers; and colored bars indicate the compositional range of the correlating tephras as given in Kimura et al. (2015).

ashes occur at Sites U1439, U1440, U1441, and U1439 and U1442, respectively (Figures 8c–8f; Table 1). Ortho- and clinopyroxenes in both tephra layers, as well as additionally some amphibole in tephra layer CIB3, as in their land equivalents, assist the correlations (e.g., Machida, 1999). Tephra layer CIB 5, which occurs at Sites U1439, U1440, and U1442, correlates with the 250 ka Onikoube-Ik tephra from Onikoube Caldera. Tephra layer CIB 7, as found at Sites U1439 and U1442, correlates with the 349 ka Naruohama-IV tephra, from an unknown source (Figures 8c–8f; Table 1). Tephra layer CIB 8, identified at Site U1440 corresponds to a 540 ka Kb-Ks tephra from South-Kyushu. This contains biotite and amphibole similar to the equivalent on land (e.g., Machida, 1999).

The above correlations indicate widespread dispersal of ash of Japan arc origin to the IBM sediments ~1,000 km away from 0.5 Ma onwards (Figures 8c–8f; Table 1). Two tephra layers, CIB 10 and CIB11 (at Sites U1441, U1442, and at Site U1439, respectively), dated at 1.95 and 2.0 Ma, correspond to the Kry1-HAS (unknown Kyushu caldera) and Bnd2-O1 (unknown North Central Japan caldera) eruptions, confirming the occurrence of older Japan-derived eruptive products in the IBM sediments (Figures 8c–8f; Table 1). Two additional marine ash layers, both from single drill sites, can also be correlated with eruptions in Japan. These are associated with unknown eruptions in Kyushu and Central Japan, at 2.4 Ma (tephra layer CIB 13, Kmz-Ngs, Site U1442) and 2.55 Ma, respectively (tephra layer CIB 16, Rih-Mn4, Site U1440) (Figures 8c–8f; Table 1). The oldest possible link (3.5 Ma) to the database of Kimura et al. (2015) is established for a marine ash bed found in Site U1440 (tephra layers CIB 18; C16), which correlates with an unknown eruption in Central Northeast Japan (Figures 8c–8f; Table 1).

Since glass compositions often overlap, especially from the same volcanic center, compositional variations with age need to be taken into account when correlating specific eruptions. As an indication of this, in Figures 8g and 8h the trace element compositions of widespread Japan tephra (Kimura et al., 2015) are plotted versus age and combined with the marine tephra data and their respective ages derived from shipboard age models. The combined geochemistry and age data strengthen our correlations based on major elements (Figures 8g and 8h).

### 8.3. Provenance and Correlations to Specific Eruptions From IBM

For the 101 ash layers recognized as originating from the IBM system, we can identify their provenance by comparing the trace element compositions of tephra with fields of compositional variation along the IBM arc, using published data (Figure 7). A similar approach has been successfully applied to understand the provenance of marine tephra of offshore Central America by utilizing regional compositional variability along the Central American volcanic arc and taking account of systematically changing subduction parameters and the nature of the incoming plate (Kutterolf et al., 2008b, 2016; Schindlbeck et al., 2016a). Our analysis assumes similar influences on the IBM subduction zone, as suggested by Tamura et al., (2009). We assume fixed relationships of the parameters controlling the along-arc variation during the entire history of the IBM system from the Oligocene to Recent, and also utilize known along-arc variations in bulk-rock and glass trace-element chemistry (Figure 9). The method is valid for both felsic and mafic tephra. If along-arc comparison is ambiguous, we favor the closest available source areas.

Along-arc geochemical variations, particularly of trace element ratios (e.g., in Ba/La, Rb/Hf, Zr/Nb and Nb/Ta; Figure 9) can successfully identify the approximate IBM arc source regions for individual tephra layers, at least for the Neogene and Quaternary time (although ratios may vary locally at any given time). Despite being less accurate than direct correlations with volcanic events and volcanic centers, which is impossible for the far-removed IBM tephra, our method represents a major step forward as it identifies source regions for eruptions where vents may be submerged or obscured by later geological events (e.g., erosion, later volcanism).

In summary, the 101 Expedition 352 marine ash layers that originated from identifiable IBM sources can be generally assigned to specific IBM regions. The Nb/Ta and Zr/Nb ratios, supported by Rb/Hf and Ba/La ratios, indicate four major IBM arc source regions (with some overlap): (1) between 27.5°N and 29°N based on high Nb/Ta, Rb/Hf and low Zr/Nb, Ba/La ratios; (2) back/rear-arc volcanism between 31°N and 32.5°N based on high Rb/Hf but only moderate Nb/Ta and low Zr/Nb ratios; (3) between 29.5°N and 31°N based on low Nb/Ta and Rb/Hf ratios; and (4) between 33.5°N and 35°N based on high Ba/La and Zr/Nb ratios (Figure 9). These correlations do not encompass the complete eruptive history of the IBM arc, for example distal



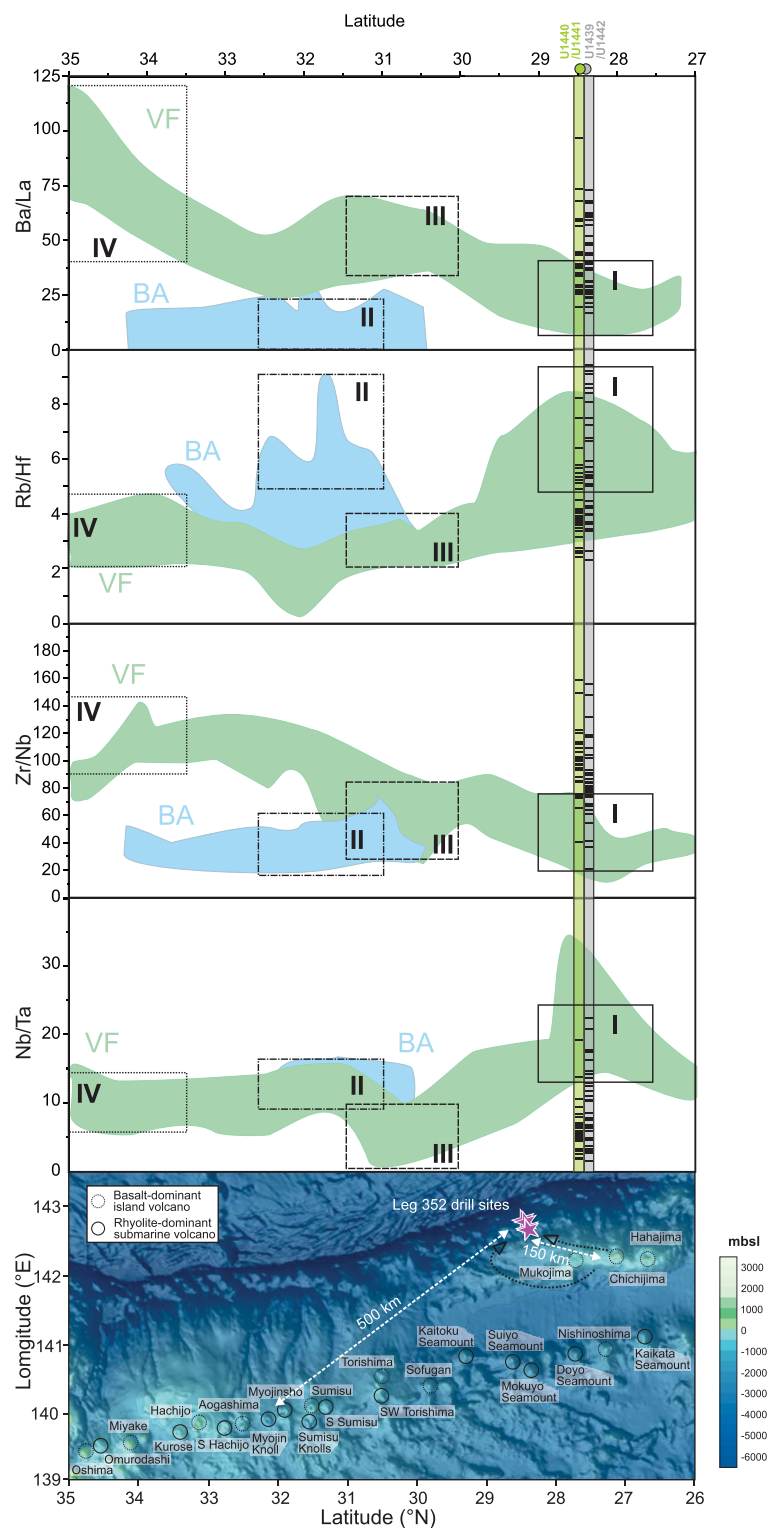


**Figure 9.** Comparison of average glass compositions of Expedition 352 tephras related to an IBM origin, with  $Ba/La$ ,  $Rb/Hf$ ,  $Zr/Nb$ , and  $Nb/Ta$  variations along the Izu-Bonin arc as discussed in the text. Distances along the arc are given in degrees latitude. The compositional groups I to IV reflect the possible origins of the marine tephras as indicated by a combination of characteristic variations along the arc. The lowermost plot shows a bathymetric map (<http://www.geomapp.org>; GMRT-Global Multi-Resolution Topography (Ryan et al., 2009), with known basaltic and rhyolitic volcanic centers along the arc and arrows indicating possible transport paths of submarine pyroclastic mass flows.

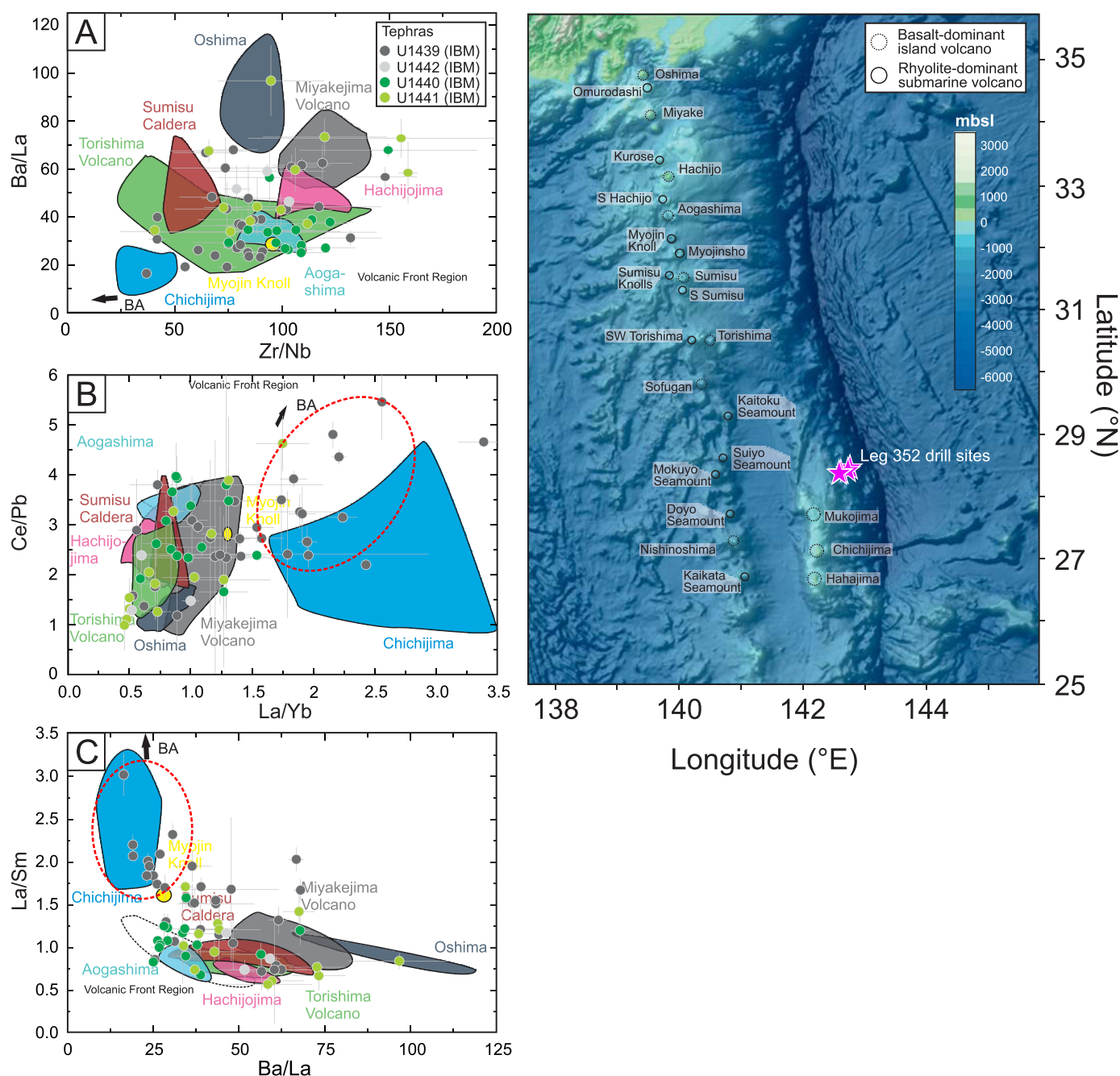


**Figure 10.** Tephra layers from Expedition 352 with an Izu-Bonin origin compared with proximal glass and bulk-rock compositions of Izu-Bonin rocks summarized from the literature. References are given in the main text. The data are averages of all of the analyses made for each individual tephra horizon. The gray bars represent the compositional range per sample. The red circles highlight Oligocene tephra layers within the diagrams, in which trace element ratios suggest a Chichijima origin. The right plot shows a bathymetric map (<http://www.geomapapp.org>; GMRT-Global Multi-Resolution Topography (Ryan et al., 2009)), with known basaltic and rhyolitic volcanic centers along the arc.

eruptions may not be recorded at the Expedition 352 drill sites; nevertheless this represents the first viable attempt to allocate the marine tephra layers of the IBM system to their host volcanic centers.

The above exploratory provenance methods can be extended and complemented by correlations with specific volcanic islands and calderas using the literature data (see above). The resulting discrimination diagrams (Figure 10) include compositional correlation fields for the volcanoes/volcanic complexes of the Izu-Bonin arc. As a result, specific correlations can be established with the Oshima, Sumisu, Torishima,

Hachijojima, Miyakejima, Agoshima, and Chichijima volcanic centers for the entire tephra inventory encompassing Oligocene to Recent time, thus extending the first-order regional provenance shown in Figure 9.

## 9. Temporal and Spatial Variations of Tephra Provenance

The overall marine sediment tephra record reflects periods of high or low abundances of ash layers from Oligocene to Pleistocene time. The tephra record starts in the Oligocene (33–24 Ma) and comprises 18 dacitic to rhyolitic ash beds that can be tentatively correlated with the compositional signals of Chichijima volcanism on the Bonin Ridge (Figures 4, 10, and 11). These ash beds differ compositionally from the Neogene and Pleistocene Izu-Bonin ash layers as they represent a transitional composition between the typical Izu-Bonin island arc signature and that of the more continentally influenced Japan arc (Figure 11), similar to the compositions found at the Kyushu-Palau-arc (e.g., Brandl et al., 2017). Since boninitic, tholeiitic, and calc-alkaline volcanism at the Bonin Ridge encompasses an age interval of ~48 to ~42 Ma (Ishizuka et al., 2006), the Oligocene marine tephra in the Expedition 352 sediments that were recovered close to the Bonin Ridge are likely to represent highly evolved late-stage Kyushu-Palau-arc volcanism in this area that has not previously recognized.

The proximity of the host volcanic centers to the depositional area supports the interpretation of the depositional textures as mass-flow deposits from submarine pyroclastic flows, with a maximum travel distance of 150–450 km (Figure 9) (e.g., Schindlbeck et al., 2013). In contrast, the air-fall tephra can be attributed to source areas that were located 100–1,300 km from the drill sites.

A significant ~9 Ma gap in volcanism is inferred in the sediments from 27 to 18 Ma during which there was no significant input of ash from either the Japan or Izu-Bonin arcs (Figure 11), probably reflecting tectonic

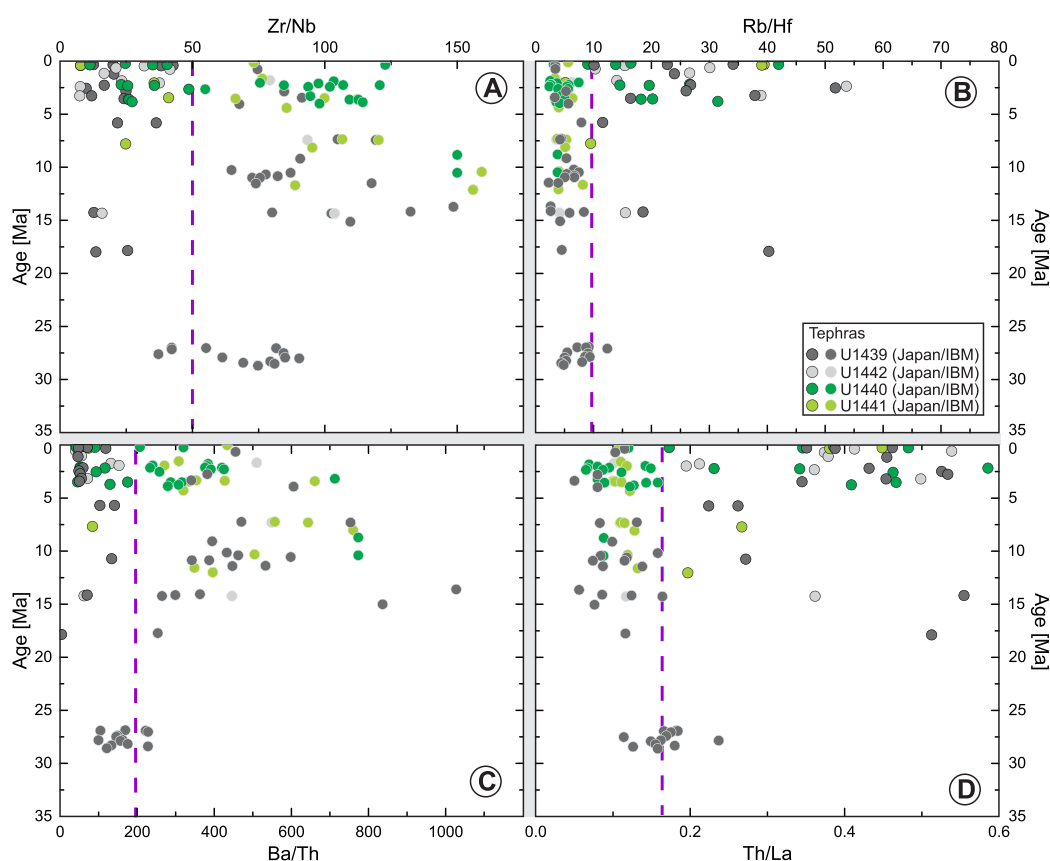


**Figure 11.** Age versus composition diagrams indicating Zr/Nb, Rb/Hf, Ba/Th, and Th/La compositional variations of the tephra inventory with time. The data represent the averages of all of the analyses made for each individual ash. Purple lines show the approximate division line between Japanese and IBM origin.

constraints (see Robertson et al., 2017). This interval coincides with the start of the backarc spreading and opening of the Shikoku Basin at  $\sim 25$  Ma, proposed by Taylor (1992), Ishizuka et al., (2011) and others, which may have limited the contribution of Izu-Bonin volcanic products. Also relevant to the pause in volcanism is the inference that Neogene North Japanese volcanism began only after 13 Ma when the initial uplift of the continental block began (Acocella et al., 2008; Ito et al., 1989; Sato, 1994; Yamamoto, 1992). Also, the distance between the source and depositional site could have become too great to be reached by tephras because the sites drifted northwards at  $\sim 30$  km/My in a N/S direction (e.g., Hall, 2002; see also Robertson et al., 2017).

From 16 to 5 Ma, the inventory is dominated by tephras of Izu-Bonin arc provenance (Figure 11). Although no clearly preferred spatial origin with time can be distinguished, large eruptions from IBM region 4 (between Agoshima and Oshima) appear to be limited to the early Pliocene to late Miocene, whereas IBM regions 2 and 3 contributed continuously to the tephra record since 16 Ma. Additionally, sporadic ash layers from the Japanese arc systems can be found in the sediments at around 12–16 Ma but become sparser with increasing age.

In contrast, at all of the Expedition 352 sites the time interval between  $\sim 5$  and 0 Ma shows an equivalent mixture of tephra sources from the (Palaeo-) Honshu and Izu-Bonin arcs (Figure 11). IBM tephras within the last 5 Ma are: (1) mainly observed on the lower forearc slope (Sites U1440 and U1441), and (2) are equally abundant as Japan-derived tephras after a sporadic occurrence in the first 2 Myr. Ash beds of Japan origin cover the entire range of source regions from Kyushu in the SW to Honshu to Hokkaido in the northeast, without any specific spatial or temporal grouping.

Low viscosity and therefore less effective fragmentation of mafic magmas normally should hinder the development of high and persistent eruption columns, a prerequisite for wide dispersion of the eruptive products (Constantini et al., 2010; Houghton et al., 2004). In contrast, the high percentage of widespread deposits from large explosive mafic eruptions in the IBM Expedition 352 sediments (15–25%) opposes this constraint and compares well with the 20% of widespread mafic ash beds found offshore in the eastern Pacific and in lacustrine sediments of Central America (Kutterolf et al., 2008b, 2016). Our research on the IBM arc reinforces earlier assumptions that abundant occurrence of widespread mafic tephras in marine sediments is characteristic of arc volcanism rather than a special seldom-occurring type of eruption, as sometimes suggested in the literature (e.g., Coltelli et al., 1998; Pérez et al., 2009).

## 10. Implications for Eruptive Volumes

In cases where data for the thickness and abundance of distal eruptive products are sparse, standard volume calculations (e.g., Fierstein & Nathenson, 1992; Pyle, 1989), based on large data sets and well-constrained isopach shapes, cannot be applied to less well-constrained and estimated distal isopachs. Where  $<20$  data points are used for isopach construction (Engwell et al., 2013), volume calculations are subject to  $>10\%$  error (Klawonn et al., 2014). However, minimum estimates of eruptive volumes can be made. Several models have been proposed to estimate tephra volumes utilizing sparse data. For example, Green et al., (2016) applied a Bayesian statistical approach to sparse proximal and distal deposits, and Sulpizio (2005) tested three empirical methods to calculate distal tephra-fall volumes. Each of these methods have been compared and tested, partly incorporating the model of Legros (2000). Here, we follow Legros's (2000) initial, simplified model that calculates a minimum tephra volume by assuming that the thickness at the farthest site lies on the dispersal axis. This assumption allows the construction of a tear-drop-shaped isopach with aperture angles of  $45^\circ$ ,  $60^\circ$ , and  $90^\circ$  (average angles for Pleistocene eruptions; e.g., Kimura et al., 2015; Machida, 2002). Then, on the resulting distribution area an exponential thickness decrease with distance from the eruptive vent has been applied (see also Kutterolf et al., 2016; Schindlbeck et al., 2016b, 2015, 2018).

Ash-bed thicknesses could vary between the Expedition 352 sites or even between the locally adjacent holes because of local or small-scale reworking or coring disturbance. However, many of the observed beds are complete and display perfect, normal gradation from medium-grained ash ( $\sim 250$   $\mu\text{m}$ ) to very fine-grained ash ( $<32$   $\mu\text{m}$ ) (Figure 3). Where a single ash bed is well-preserved at several sites its original maximum thickness can be confidently determined. This can then be taken as the "true" thickness of that particular ash layer in the region even if correlative ash layers in other sites are thinner.



The majority of the marine tephra layers assigned to a Japanese provenance are assumed to have come from Kyushu. The approximate volume estimates for these eruptions (assuming an intermediate distribution fan opening angle of  $60^\circ$  similar to Schindlbeck et al., 2018) vary between  $\sim 35$  and  $\sim 49$  km<sup>3</sup> tephra volume ( $17\text{--}23$  km<sup>3</sup> DRE; CIB 7, 8, 10, 13; 1.5–2 cm ash layer thickness; Table 1; supporting information Table S3). This confirms the preliminary volume estimates of  $>100$  km<sup>3</sup> for the Kobayashi-Ks (Kb-Ks) eruption (CIB8;  $38\text{--}72$  km<sup>3</sup> tephra volume) according to Machida and Arai (2003). Two notable exceptions are seen for Kyushu eruptions: Ata-Th (CIB 3; 13 cm ash layer thickness) and Aso-1 (CIB4; 6 cm ash layer thickness) imply eruptive tephra volumes of  $\sim 300$  km<sup>3</sup> ( $\sim 143$  km<sup>3</sup> DRE) and  $\sim 140$  km<sup>3</sup> ( $66$  km<sup>3</sup> DRE), respectively (Table 1; supporting information Table S3). The ash layer thickness of 83 cm of the Ata-Th tephra at Site U1440 could be due to local thickening, drilling disturbance (flow in of ash matter; e.g., Jutzeler et al., 2014), or both. If, however, the thickness is primary, the eruptive volume would increase to  $\sim 1,900$  km<sup>3</sup>, which seems to be excessive. Our results corroborate and extend the initial tephra volume estimates of  $\gg 150$  km<sup>3</sup> for Ata-Th and of  $\gg 50$  km<sup>3</sup> for Aso-1, as given by Machida (2002). Late Pliocene and Early Pleistocene eruptions from Central Japan (CIB 11, 16, and 18; 3–10 cm ash layer thickness) account for  $\sim 40$  to  $\sim 150$  km<sup>3</sup> tephra volume ( $20\text{--}70$  km<sup>3</sup> DRE), Nanko I from SW Japan (CIB 1; 4 cm) results in  $\sim 90$  km<sup>3</sup> ( $44$  km<sup>3</sup> DRE), whereas eruptions in NE-Japan reached volumes of  $\sim 16$  km<sup>3</sup> for BT51 ( $\sim 8$  km<sup>3</sup> DRE; CIB 2; 1 cm ash layer thickness) and  $\sim 350$  km<sup>3</sup> for Onikoube-IK ( $\sim 160$  km<sup>3</sup> DRE; CIB 5; 16 cm ash layer thickness) (Table 1; supporting information Table S3).

Although we are unable to correlate known individual eruptions along the Izu-Bonin arc with the marine tephra layers investigated in this study, we can at least assign average compositions to the known eruptive centers along the subduction zone. Using average ash layer thicknesses and simple distribution models for sub-aerial ash fallouts (Legros, 2000), an initial volume estimate can be made for eruptions that reached the atmosphere from the respective areas. However, we cannot exclude the possibility that voluminous submarine eruptions also occurred but did not reach distal areas (e.g., Schindlbeck et al., 2018). For the most proximal IBM region 1, between Chichijima and Mukojima ( $\sim 150$  km distance from source), the minimum distribution area (up to 10 cm isopach) is calculated as  $\sim 1 \times 10^5$  km<sup>2</sup> with a tephra volume of  $3\text{--}5$  km<sup>3</sup> ( $1\text{--}2$  km<sup>3</sup> DRE) (Table 1; supporting information Table S3). For IBM region 2 (backarc) and region 3 (volcanic front),  $\sim 300$  km or  $\sim 450$  km from the Expedition 352's depositional area, tephra volumes of  $\sim 9$  to  $\sim 17$  km<sup>3</sup> ( $4\text{--}8$  km<sup>3</sup> DRE) and  $\sim 4$  to  $\sim 9$  km<sup>3</sup> ( $2\text{--}4$  km<sup>3</sup> DRE) are calculated when considering minimum distribution areas of  $\sim 7 \times 10^5$  km<sup>2</sup> and  $\sim 3 \times 10^5$  km<sup>2</sup>, respectively, at an average ash layer thicknesses of  $\sim 4$  cm (Table 1; supporting information Table S3). IBM region 4, up to 750 km away from the Expedition 352 depositional area, was the source of the largest eruptions recorded in the Expedition 352 IBM sediments. The eruptions potentially produced  $21\text{--}40$  km<sup>3</sup> ( $10\text{--}19$  km<sup>3</sup> DRE) of tephra, derived from minimum distribution areas of  $\sim 2 \times 10^6$  km<sup>2</sup> with ash layer thicknesses of 1–42 cm (Table 1).

In summary, volumetric eruption magnitudes ( $M_v = \log_{10}(V) - 4$ , where  $V$  (m<sup>3</sup>) represent tephra volume, (Pyle, 1995) (equivalent to the VEI index of Newhall & Self, 1982), as derived from first-order volume estimates, generally range from  $M_v = 6.4\text{--}7.7$  for tephra layers that correlate with Japan eruptions, whereas our rough estimates of eruptive products originating in the four different IBM regions range between  $M_v = 5.7$  and  $6.6$ . The distal ash layers in the IBM forearc sediments therefore help us to constrain the size of some IBM and Japan eruptions, increase the previous volume and magnitude estimates for known Japan eruptions (Table 1), and demonstrate how important distal deposits are for the characterization of large explosive eruptions.

## 11. Conclusions

We have established a tephrochronostratigraphy for IODP Expedition 352 IBM forearc sediments, which highlights the occurrence of large Oligocene to Pleistocene explosive eruptions related to the Japan and IBM arcs. Of the 157 confirmed ash horizons recovered, 101 ash layers within the entire time frame (Oligocene–Recent) can be allocated to an IBM origin, whereas 56 ash layers from the Pleistocene to early Miocene have a Japan provenance. The characteristics of distinctive ash beds allow 24 site-to-site correlations of widespread major tephra layers, thereby providing tie points in the sedimentary sequence. The overall evidence also facilitates 12 correlations between the tephra layers in the marine sediments and specific eruptions from Kyushu, Central Japan (S- to Central Honshu) and North Japan (N-Honshu to Hokkaido), with ages 115

ka to 3.5 Ma. Additionally, four IBM arc provenance regions have been established for Oligocene to Pleistocene tephra based on along-arc compositional variations.

An initial comprehensive tephrochronostratigraphy for the entire Japanese and Izu-Bonin region is established using a combination of correlations between the drill sites and their independently dated terrestrial counterparts, along-arc provenance, and the biostratigraphic ages of marine sediments recovered during Expedition 352. Additionally, we provide a stratigraphically classified tephra database of glass compositions for large-magnitude Quaternary and Neogene explosive eruptions as a basis for further correlations with marine tephra archives in the region.

Using correlations with individual eruptions in Japan, we have also estimated respective eruptive volumes and eruption magnitudes. When the marine tephra are assigned to provenance regions within the Izu-Bonin arc system, it becomes clear just how large eruptions from the source regions must have been to reach the drill sites. The tephra inventory additionally provides glimpses of the history of explosive volcanism on the Izu-Bonin arc system back to the Oligocene and also helps to indicate how this relates to explosive volcanism in Japan.

### Acknowledgments

We are extremely grateful to the crew of the *JOIDES Resolution* and to TAMU who made Expedition 352 so successful. The International Ocean Discovery Program provided shipboard data and samples. This project was mainly funded by the German Research Foundation (DFG) with grants KU2685/4-1 and SCH1349/1-1. AHFR's input was financially supported by an IODP research grant from the UK Natural Environmental Council (Postcruise grant COL-T352A13). A.T.B. was supported by funds from an ARC LIEF grant (ARC - LE160100067) awarded to the Australia New Zealand IODP Consortium (ANZIC). K.P. was supported by the IODP-JR50 and an NSF/USSSP postcruise grant (COL-T352A13). For preparation of the tephra in the laboratory and assistance with the chemical analyses, we thank Kai Fockenberg, Fuo Lung Lin, and Mario Thöner. Finally we thank Editor J. Feinberg for the handling and editing of the manuscript and an anonymous reviewer for helpful reviews that strengthened the paper. All geochemical data and volume calculations are given in the supporting information Data Set S1–S4.

### References

- Acocella, V., Yoshida, T., Yamada, R., & Funicello, F. (2008). Structural control on late Miocene to Quaternary volcanism in the NE Honshu arc, Japan. *Tectonics*, 27, TC5008. <https://doi.org/10.1029/2008TC002296>
- Amma-Miyasaka, M., & Nakagawa, M. (1998). Recent magma plumbing system beneath Miyakejima volcano, Izu islands, inferred from petrological study of the 1940 and 1962 lavas. *Bulletin of the Volcanological Society of Japan*, 43, 433–455.
- Arculus, R. J., Arculus, R. J., Ishizuka, O., Bogus, K. A., Gurnis, M., Hickey-Vargas, R., . . . Zhang, Z. (2015). A record of spontaneous subduction initiation in the Izu-Bonin-Mariana arc. *Nature Geoscience*, 8(9), 728–733.
- Arculus, R. J., & Bloomfield, A. L. (1992). Major-element geochemistry of ashes from Sites 782, 784, and 786 in the Bonin forearc. In P. Fryer et al. (Eds.), *Proceedings of the Ocean Drilling Program: Scientific results* (Vol. 126, pp. 277–292). College Station, TX: Ocean Drilling Program.
- Arima, M., & R. J. (1997). The Izu-Bonin-Mariana (IBM) arc system: Outstanding natural laboratory for the studies of convergent plate margins. *JAMSTEC Journal of Deep Sea Research, Special Volume*, 17–19.
- Bloomer, S. H., Taylor, B., MacLeod, C. J., Stern, R., Fryer, J. P., Hawkins, J. W., & Johnson, L. (1995). Early arc volcanism and the ophiolite problem: A perspective from drilling in the western Pacific. In B. Taylor & J. Natland (Eds.), *Active margins and marginal basins of the western Pacific, Geophysical Monograph Series* (Vol. 88, pp. 1–30). Washington, DC: American Geophysical Union.
- Brandl, P. A., Hamada, M., Arculus, R. J., Johnson, K., Marsaglia, K. M., Savov, I. P., . . . Li, H. (2017). The arc arises: The links between volcanic output, arc evolution and melt composition. *Earth and Planetary Science Letters*, 461, 73–84. <https://doi.org/10.1016/j.epsl.2016.12.027>
- Bryant, C. J., Arculus, R. J., & Eggins, S. M. (1999). Laser ablation-inductively coupled plasma-mass spectrometry and tephra: A new approach to understanding arc-magma genesis. *Geology*, 27, 1119–1122.
- Bryant, C. J., Arculus, R. J., & Eggins, S. M. (2003). The geochemical evolution of the Izu-Bonin arc system: A perspective from tephra recovered by deep-sea drilling. *Geochemistry, Geophysics, Geosystems*, 4(11), 1094. <https://doi.org/10.1029/2002GC000427>
- Bukry, D. (1973). Low-latitude coccolith biostratigraphic zonation, *Initial Reports Deep Seas Drilling Project*, 15, 685–703.
- Bukry, D. (1975). Coccolith and silicoflagellate stratigraphy, northwestern Pacific Ocean, Deep Sea Drilling Project Leg 32, *Initial Reports Deep Seas Drilling Project*, 32, 677–701.
- Carey, S., & Sigurdsson, H. (2000). Grain size of Miocene volcanic ash layers from Sites 998, 999, and 1000: Implications for source areas and dispersal. In R. M. Leckie et al. (Eds.), *Proceedings of the Ocean Drilling Program: Scientific results* (Vol. 165, pp. 101–110). College Station, TX: Ocean Drilling Program.
- Carey, S. N. (2000). Volcaniclastic sedimentation around island arcs. In H. Sigurdsson et al. (Eds.), *Encyclopedia of volcanoes* (2nd ed., pp. 627–642). London, UK: Academic Press.
- Clift, P. D., & Blusztajn, J. (1999). The trace-element characteristics of Aegean and Aeolian volcanic arc marine tephra. *Journal of Volcanology and Geothermal Research*, 92, 321–347.
- Coltelli, M., Del Carlo, P., & Vezzoli, L. (1998). Discovery of a Plinian basaltic eruption of Roman age at Etna volcano, Italy. *Geology*, 26, 1095–1098.
- Constantini, L., Houghton, B. F., & Bonadonna, C. (2010). Constraints on eruption dynamics of basaltic explosive activity derived from chemical and microtextural study: The example of the Fontana Lapilli Plinian eruption, Nicaragua. *Journal of Volcanology and Geothermal Research*, 189, 207–224.
- Cosca, M., Arculus, R. J., Pearce, J., & Mitchell, J. (1998). 40Ar/39Ar and K–Ar geochronological age constraints for the inception and early evolution of the Izu-Bonin-Mariana arc system. *Island Arc*, 7(3), 579–595.
- De Wever, P., Dumitrica, P., & Chaulet, J. P. (2001). *Radiolarians in the sedimentary record* (524 p.). Amsterdam, the Netherlands: Gordon and Breach.
- Engwell, S., Sparks, R., & Aspinall, W. (2013). Quantifying uncertainties in the measurement of tephra fall thickness. *Journal of Applied Volcanology*, 2(1), 1.
- Fierstein, J., & Nathenson, M. (1992). Another look at the calculation of fallout tephra volumes. *Bulletin of Volcanology*, 54, 156–167.
- Fiske, R. S., Naka, J., Iizasa, K., Yuasa, M., & Klaus, A. (2001). Submarine silicic caldera at the front of the Izu-Bonin arc, Japan: Voluminous sea-floor eruptions of rhyolite pumice. *Geological Society of America Bulletin*, 113, 813–824.
- Fujioka, K., Matsuo, Y., Nishimura, A., Koyama, M., & Rodolfo, K. S. (1992). Tephra of the Izu-Bonin Forearc (Sites 787, 792 and 793). In B. Taylor et al. (Eds.), *Proceedings of the Ocean Drilling Program: Scientific results* (Vol. 126, pp. 47–74). College Station, TX: Ocean Drilling Program. <https://doi.org/10.2973/odp.proc.sr.126.117.1992>
- Gill, J., Hiscott, R., & Vidal, P. (1994). Turbidite geochemistry and evolution of the Izu-Bonin arc and continents. *Lithos*, 33(1), 135–168.
- Gill, J., Seales, C., Thompson, P., Hochstaedter, A., & Dunlap, C. (1992). Petrology and geochemistry of Pliocene-Pleistocene volcanic rocks from the Izu Arc, Leg 126. In B. Taylor et al. (Eds.), *Proceedings of the Ocean Drilling Program: Scientific results*, (Vol. 126, pp. 383–404). College Station, TX: Ocean Drilling Program. <https://doi.org/10.2973/odp.proc.sr.126.145.1992>

- Gorton, M. P., & Schandl, E. S. (2000). From continents to island arcs: A geochemical index of tectonic setting for arc-related and within-plate felsic to intermediate volcanic rocks. *The Canadian Mineralogist*, 38(5), 1065–1073.
- Gradstein, F. M., Ogg, J., Schmitz, G. M., & Ogg, G. (Eds.) (2012). *The geologic time scale 2012* (1176 pp.). Amsterdam, the Netherlands: Elsevier.
- Green, R. M., Bebbington, M. S., Jones, G., Cronin, S. J., & Turner, M. B. (2016). Estimation of tephra volumes from sparse and incompletely observed deposit thicknesses. *Bulletin of Volcanology*, 78(4), 1–18.
- Günther, D., Jackson, S. E., & Longerich, H. P. (1999). Laser ablation and arc/spark solid sample introduction into inductively coupled plasma mass spectrometers. *Spectrochimica Acta Part B: Atomic Spectroscopy*, 54(3), 381–409.
- Hall, C. E., Gurnis, M., Sdrolias, M., Lavie, L. L., & Müller, R. D. (2003). Catastrophic initiation of subduction following forced convergence across fracture zones. *Earth and Planetary Science Letters*, 212(1), 15–30.
- Hall, R. (2002). Cenozoic geological and plate tectonic evolution of SE Asia and the SW Pacific: Computer-based reconstructions, model and animations. *Journal of Asian Earth Sciences*, 20(4), 353–431.
- Hamada, M., & Fujii, N. (2007). H<sub>2</sub>O-rich island arc low-K tholeiite magma inferred from Ca-rich plagioclase melt inclusion equilibria. *Geochemical Journal*, 41, 437–461.
- Hirose, K., Nagahashi, Y., & Nakazawa, N. (2014). Lithostratigraphy and dating of lacustrine sediment core (INW2012) from Lake Inawashiro-ko, Fukushima Prefecture, Japan. *The Quaternary Research (Daiyonki-Kenkyu)*, 53(3), 157–173.
- Hochstaedter, A., Gill, J., Peters, R., Broughton, P., Holden, P., & Taylor, B. (2001). Across-arc geochemical trends in the Izu-Bonin arc: Contributions from the subducting slab. *Geochemistry, Geophysics, Geosystems*, 2(7), 1019. <https://doi.org/10.1029/2000GC000105>
- Houghton, B. F., Wilson, C. J. N., Del Carlo, P., Coltelli, M., Sable, J. E., & Carey, R. (2004). The influence of conduit processes on changes in style of basaltic Plinian eruptions: Tarawera 1886 and Etna 122 BC. *Journal of Volcanology and Geothermal Research*, 137, 1–14.
- Hunt, J. B., & Hill, P. G. (2001). Tephrological implications of beam size-sample-size effects in electron microprobe analysis of glass shards. *Journal of Quaternary Science*, 16(2), 105–117.
- Ikehara, K. (2015). Marine tephra in the Japan Sea sediments as a tool for paleoceanography and paleoclimatology. *Progress in Earth and Planetary Science*, 2(1), 36.
- Ishizuka, O., Kimura, J.-I., Lic, Y. B., Sternd, R. J., Reagane, M. K., Taylor, R. N., . . . Haraguchi, S. (2006). Early stages in the evolution of Izu-Bonin arc volcanism: New age, chemical, and isotopic constraints. *Earth and Planetary Science Letters*, 250, 385–401.
- Ishizuka, O., Tani, K., Reagane, M., Kanayama, K., Umino, S., Harigane, Y., . . . Dunkley, D. (2011). The timescales of subduction initiation and subsequent evolution of an oceanic island arc. *Earth and Planetary Science Letters*, 306(3), 229–240.
- Ishizuka, O., Taylor, R. N., Yuasa, M., Milton, J. A., Nesbitt, R. W., Uto, K., & Sakamoto, I. (2007). Processes controlling along-arc isotopic variation of the southern Izu-Bonin arc. *Geochemistry, Geophysics, Geosystems*, 8, Q06008. <https://doi.org/10.1029/2006GC001475>
- Ito, T., Utada, M., & Okuyama, T. (1989). Mio-Pliocene calderas in the Backbone Region in northeast Japan. *Memoirs of the Geological Society of Japan*, 32, 409–429.
- Jutzeler, M., White, J. D. L., Talling, P. J., McCanta, M., Morgan, S., Le Friant, A., & Ishizuka, O. (2014). Coring disturbances in IODP piston cores with implications for offshore record of volcanic events and the Missoula megafloods. *Geochemistry, Geophysics, Geosystems*, 15, 3572–3590. <https://doi.org/10.1002/2014GC005447>
- Kamikuri, S.-I., Motoyama, I., Nishi, H., & Iwai, M. (2009). Evolution of Eastern Pacific Warm Pool and upwelling processes since the middle Miocene based on analysis of radiolarian assemblages: Response to Indonesian and Central American Seaways. *Palaeogeography, Palaeoclimatology, Palaeoecology*, 280(3), 469–479.
- Keller, J., Ryan, W. B. F., Ninkovich, D., & Altherr, R. (1978). Explosive volcanic activity in the Mediterranean over the past 200,000 years as recorded in deep-sea sediments. *Geological Society of America Bulletin*, 89, 591–604.
- Kimura, J.-I., Kent, A. J. R., Rowe, M. C., Katakuse, M., Nakano, F., Hacker, B. R., . . . Stern, R. J. (2010). Origin of cross-chain geochemical variation in Quaternary lavas from the northern Izu arc: Using a quantitative mass balance approach to identify mantle sources and mantle wedge processes. *Geochemistry, Geophysics, Geosystems*, 11, Q10011. <https://doi.org/10.1029/2010GC003050>
- Kimura, J. I., Nagahashi, Y., Satoguchi, Y., & Chang, Q. (2015). Origins of felsic magmas in Japanese subduction zone: Geochemical characterizations of tephra from caldera-forming eruptions < 5 Ma. *Geochemistry, Geophysics, Geosystems*, 16, 2147–2174. <https://doi.org/10.1002/2015GC005854>
- Klawonn, M., Houghton, B. F., Swanson, D. A., Fagents, S. A., Wessel, P., & Wolfe, C. J. (2014). Constraining explosive volcanism: Subjective choices during estimates of eruption magnitude. *Bulletin of Volcanology*, 76(2), 1–6.
- Kutterolf, S., Freundt, A., & Burkert, C. (2011). Eruptive history and magmatic evolution of the 1.9 kyr Plinian dacitic Chiltepe Tephra from Apoyeque volcano in west-central Nicaragua. *Bulletin of Volcanology*, 73, 811–831.
- Kutterolf, S., Freundt, A., & Pérez, W. (2008a). The Pacific offshore record of Plinian arc volcanism in Central America, part 2: Tephra volumes and erupted masses. *Geochemistry, Geophysics, Geosystems*, 9, Q02502. <https://doi.org/10.1029/2007GC001791>
- Kutterolf, S., Freundt, A., Pérez, W., Mörz, T., Schacht, U., Wehrmann, H., & Schmincke, H.-U. (2008b). The Pacific offshore record of Plinian arc volcanism in Central America, part 1: Along-arc correlations. *Geochemistry, Geophysics, Geosystems*, 9, Q02501. <https://doi.org/10.1029/2007GC001631>
- Kutterolf, S., Freundt, A., Schacht, U., Bürk, D., Harders, R., Mörz, T., & Pérez, W. (2008c). The Pacific offshore record of Plinian arc volcanism in Central America, part 3: Application to forearc geology. *Geochemistry, Geophysics, Geosystems*, 9, Q02503. <https://doi.org/10.1029/2007GC001826>
- Kutterolf, S., Jegen, M., Mitrovica, J. X., Kwasnitschka, T., Freundt, A., & Huybers, P. (2013). A detection of Milankovitch frequencies in global volcanic activity. *Geology*, 41(2), 227–230.
- Kutterolf, S., Liebetrau, V., Moerz, T., Freundt, A., Hammerich, T., & Garbe-Schönberg, D. (2008d). Lifetime and cyclicity of fluid venting at forearc mound structures determined by tephrostratigraphy and radiometric dating of authigenic carbonates. *Geology*, 36(9), 707–710.
- Kutterolf, S., Schindlbeck, J. C., Anselmetti, F. S., Ariztegui, D., Brenner, M., Curtis, J., . . . Wang, K.-L. (2016). A 400-ka tephrochronological framework for Central America from Lake Petén Itzá (Guatemala) sediments. *Quaternary Science Reviews*, 150, 200–220.
- Ledbetter, M. T. (1985). Tephrochronology of marine tephra adjacent to Central America. *Geological Society of America Bulletin*, 96, 77–82.
- Legros, F. (2000). Minimum volume of a tephra fallout deposit estimated from a single isopach. *Journal of Volcanology and Geothermal Research*, 96(1), 25–32.
- Le Maitre, R. W., Streckeis, A., Zanettin, B., Le Bas, M. J., Bonin, B., & Bateman, P. (2002). *Igneous rocks: A classification and glossary of terms*. Cambridge, UK: Cambridge University Press.
- Lowe, D. J. (2011). Tephrochronology and its application: A review. *Quaternary Geochronology*, 6, 107–153.
- Lowe, D. J., Shane, P. A. R., Alloway, B. V., & Newnham, E. M. (2008). Fingerprints and age models for widespread New Zealand tephra marker beds erupted since 30,000 years ago: A framework for NZ-INTIMATE. *Quaternary Science Reviews*, 27, 95–126.
- Machida, H. (1999). The stratigraphy, chronology and distribution of distal marker-tephras in and around Japan. *Global and Planetary Change*, 21, 71–94.

- Machida, H. (2002). Volcanoes and tephra in the Japan area. *Global Environmental Research-English Edition*, 6(2), 19–28.
- Machida, H., & Arai, F. (2003). *Atlas of tephra in and around Japan* (336pp.) [in Japanese]. Tokyo: Tokyo University Press.
- Martini, E. (1971). *Standard tertiary and quaternary calcareous nannoplankton zonation*. Paper presented at Proceedings of the Second Planktonic Conference (pp. 739–785), Roma 1970, Tecnoscienza.
- Miller, M., Kennett, B., & Toy, V. (2006). Spatial and temporal evolution of the subducting Pacific plate structure along the western Pacific margin. *Journal of Geophysical Research*, 111, B02401. <https://doi.org/10.1029/2005JB003705>
- Moriwaki, H., Westgate, J. A., Sandhu, A. S., Preece, S. J., & Arai, F. (2008). New glass fission-track ages of Middle Pleistocene tephra on Yakushima Island, southern Japan. *Quaternary International*, 178(1), 128–137.
- Müller, R. D., Seton, M., Zahirovic, S., Williams, S. E., Matthews, K. J., Wright, N. M., . . . Hosseinpour, M. (2016). Ocean basin evolution and global-scale plate reorganization events since Pangea breakup. *Annual Review of Earth and Planetary Sciences*, 44, 107–138.
- Nagahashi, Y., & Kataoka, S. (2014). Tephrology (part 5): Major element composition of volcanic glass shards and tephra beds correlation. *The Quaternary Research (Daiyonki-Kenkyu)*, 53(5), 265–270.
- Nagahashi, Y., Yoshikawa, S., Miyakawa, C., Uchiyama, T., & Inouchi, Y. (2004). Stratigraphy and Chronology of Widespread Tephra Layers during the Past 430ky in the Kinki District and the Yatsugatake Mountains. *The Quaternary Research (Daiyonki-Kenkyu)*, 43(1), 15–35.
- Nagahashi, Y., Yoshida, T., Nakai, S., & Okudaira, T. (2003). Evaluation and correction of EDS results of the glass shards from some representative tephra by comparison with XRF analysis. *The Quaternary Research (Daiyonki-Kenkyu)*, 42(4), 265–277.
- Nakajima, S., Shuto, K., Kagami, H., Ohki, J., & Itaya, T. (1995). Across-arc chemical and isotopic variation of late Miocene to Pliocene volcanic rocks from the northern Japan arc. *Memoir of the Geological Society of Japan*, 44, 197–226.
- Nakano, S., & Yamamoto, T. (1987). Major element chemistry of the products of the 1986 eruption of Izu-Oshima volcano. *Bulletin of the Geological Survey of Japan*, 38, 631–647.
- Newhall, C. G., & Self, S. (1982). The volcanic explosivity index (VEI): An estimate of explosive magnitude for historical volcanism. *Journal of Geophysical Research*, 87(C2), 1231–1238.
- Norman, M., Pearson, N., Sharma, A., & Griffin, W. (1996). Quantitative analysis of trace elements in geological materials by laser ablation ICPMS: Instrumental operating conditions and calibration values of NIST glasses. *Geostandards Newsletter*, 20(2), 247–261.
- Okada, H., & Bukry, D. (1980). Supplementary modification and introduction of code numbers to the low-latitude coccolith biostratigraphic zonation (Bukry, 1973; 1975). *Marine Micropaleontology*, 5, 321–325.
- Okino, K., Matsuda, K., Christie, D. M., Nogi, Y., & Koizumi, K. I. (2004). Development of oceanic detachment and asymmetric spreading at the Australian-Antarctic Discordance. *Geochemistry, Geophysics, Geosystems*, 5, Q12012. <https://doi.org/10.1029/2004GC000793>
- Patino, L. C., Carr, M. J., & Feigenson, M. D. (2000). Local and regional variations in Central American arc lavas controlled by variations in subducted sediment input. *Contributions to Mineralogy and Petrology*, 138(3), 265–283.
- Pearce, J. A., Reagan, M. K., Stern, R. J., & Petronotis, K. (2013). Izu-Bonin-Mariana fore arc: Testing subduction initiation and ophiolite models by drilling the outer Izu-Bonin-Mariana fore arc. *Integrated Ocean Drilling Program: Scientific Prospectus*, 352. <https://doi.org/10.14379/iodp.pr.352.2015>
- Pearce, N. J. G., Denton, J. S., Perkins, W. T., Westgate, J. A., & Alloway, B. V. (2007). Correlation and characterization of individual glass shards from tephra deposits using trace element laser ablation ICPMS analyses: current status and future potential. *Journal of Quaternary Science*, 22, 721–736.
- Pearce, N. J. G., Westgate, J. A., Perkins, W. T., Eastwood, W. J., & Shane, P. (1999). The application of laser ablation ICP-MS to the analysis of volcanic glass shards from tephra deposits: Bulk glass and single shard analysis. *Global and Planetary Change*, 21, 151–171.
- Pérez, W., Freundt, A., Kutterolf, S., & Schmincke, H.-U. (2009). The Masaya Triple Layer: A 2100 year old basaltic multi-episodic Plinian eruption from the Masaya Caldera Complex (Nicaragua). *Journal of Volcanology and Geothermal Research*, 179(3–4), 191–205.
- Plank, T. (2001). *Subduction factory input and output* (report, pp. 73–77). Boston, MA: Department of Earth Sciences.
- Pyle, D. M. (1989). The thickness, volume and grain size of tephra fall deposits. *Bulletin of Volcanology*, 51, 1–15.
- Pyle, D. M. (1995). Mass and energy budgets of explosive volcanic eruptions. *Geophysical Research Letters*, 22(5), 563–566.
- Reagan, M. K., Ishizuka, O., Stern, R. J., Kelley, K. A., Ohara, Y., Blichert-Toft, J., . . . Woods, M. (2010). Fore-arc basalts and subduction initiation in the Izu-Bonin-Mariana system. *Geochemistry, Geophysics, Geosystems*, 11, Q03X12. <https://doi.org/10.1029/2009GC002871>
- Reagan, M. K., Pearce, J. A., Petronotis, K., Almeev, R. R., Avery, A. J., Carvalho, C., . . . Whattam, S. A. (2017). Subduction initiation and ophiolite crust: New insights from IODP drilling. *International Geology Review*, 1–12.
- Reagan, M. K., Pearce, J. A., Petronotis, K., & Scientists, E. (2015). Izu-Bonin-Mariana fore arc. In *Proceedings of the International Ocean Discovery Program* (Vol. 352). College Station, TX: International Ocean Discovery Program. <https://doi.org/10.14379/iodp.proc.14352.12015>
- Robertson, A. H. F., Kutterolf, S., Avery, A. J., Baxter, A. T., Petronotis, K., Acton, G. D., . . . Schindlbeck, J. C. (2017). Depositional setting, provenance and tectonic-volcanic setting of Eocene-Recent deep-sea sediments of the oceanic Izu-Bonin forearc, NW Pacific (IODP Expedition 352). *International Geology Review*, 1–39. <https://doi.org/10.1080/00206814.2017.1393634>
- Rodolfo, K. S., Solidum, R. U., Nishimura, A., Matsuo, Y., & Fujioka, K. (1992). Major-Oxide stratigraphy of glass shards in volcanic ash layers of the Izu-Bonin Arc-backarc sites (Sites 788/789 and 790/791). In B. Taylor et al. (Eds.), *Proceedings of the Ocean Drilling Program: Scientific results* (Vol. 126). College Station, TX: Ocean Drilling Program.
- Ryan, J. G., Shervais, J. W., Li, Y., Reagan, M. K., Li, H. Y., Heaton, D., . . . the IODP Expedition 352 Scientific Team (2017). Application of a handheld X-ray fluorescence spectrometer for real-time, high-density quantitative analysis of drilled igneous rocks and sediments during IODP Expedition 352. *Chemical Geology*, 451, 55–66.
- Ryan, W. B. F., Carbotte, S. M., Coplan, J. O., O'Hara, S., Melkonian, A., Arko, R., . . . Zemsky, R. (2009). Global multi-resolution topography synthesis. *Geochemistry, Geophysics, Geosystems*, 10, Q03014. <https://doi.org/10.1029/2008GC002332>
- Sato, H. (1994). The relationship between late Cenozoic tectonic events and stress field and basin development in northeast Japan. *Journal of Geophysical Research*, 99(B11), 22261–22274.
- Satoguchi, Y., & Nagahashi, Y. (2012). Tephrostratigraphy of the Pliocene to middle Pleistocene series in Honshu and Kyushu Islands, Japan. *Island Arc*, 21, 149–169. <https://doi.org/10.1111/j.1440-1738.2012.00816.x>
- Schindlbeck, J. C., Kutterolf, S., Freundt, A., Alvarado, G. E., Wang, K. L., Straub, S. M., . . . Woodhead, J. D. (2016a). Late Cenozoic tephrostratigraphy offshore the southern Central American Volcanic Arc: 1. Tephra ages and provenance. *Geochemistry, Geophysics, Geosystems*, 17, 4641–4668. <https://doi.org/10.1002/2016GC006503>
- Schindlbeck, J. C., Kutterolf, S., Freundt, A., Andrews, G., Wang, K.-L., Völker, D., . . . Hoernle, K. (2016b). Alkaline marine tephra layers at ODP Site 1241-Major explosive eruptions from an oceanic volcano in a pre-shield stage? *Journal of Volcanology and Geothermal Research*, 328, 96–104.
- Schindlbeck, J. C., Kutterolf, S., Freundt, A., Scudder, R. P., Pickering, K. T., & Murray, R. W. (2013). Emplacement processes of submarine volcanoclastic deposits (IODP Site C0011, Nankai Trough). *Marine Geology*, 343, 115–124.



- Schindlbeck, J. C., Kutterolf, S., Freundt, A., Straub, S., Vannucchi, P., & Alvarado, G. (2016c). Late Cenozoic tephrostratigraphy offshore the southern Central American Volcanic Arc: 2. Implications for magma production rates and subduction erosion. *Geochemistry, Geophysics, Geosystems*, 17, 4585–4604. <https://doi.org/10.1002/2016GC006504>
- Schindlbeck, J. C., Kutterolf, S., Freundt, A., Straub, S. M., Wang, K.-L., Jegen, M., . . . Sandoval, M. I. (2015). The Miocene Galápagos ash layer record of Integrated Ocean Drilling Program Legs 334 and 344: Ocean-island explosive volcanism during plume-ridge interaction. *Geology*, 43(7), 599–602.
- Schindlbeck, J. C., Kutterolf, S., Straub, S., Andrews, G., & Wang, K.-L. (2018). The 1 Ma-recent tephra record at IODP Sites U1436 and U1437: Insights into explosive volcanism from the Japan and Izu arcs. *Island Arc*. <https://doi.org/10.1111/iar.12244>
- Scudder, R. P., Murray, R. W., Schindlbeck, J. C., Kutterolf, S., Hauff, F., Underwood, M. B., . . . McKinley, C. C. (2016). Geochemical approaches to the quantification of dispersed volcanic ash in marine sediment. *Progress in Earth and Planetary Science*, 3(1), 1–32.
- Shukuno, H., Tamura, Y., Tani, K., Chang, Q., Suzuki, T., & Fiske, R. (2006). Origin of silicic magmas and the compositional gap at Sumisu submarine caldera, Izu-Bonin arc, Japan. *Journal of Volcanology and Geothermal Research*, 156(3), 187–216.
- Stern, R. J. (2004). Subduction initiation: Spontaneous and induced. *Earth and Planetary Science Letters*, 226, 275–292.
- Stern, R. J., Fouch, M. J., & Klempner, S. L. (2003). An overview of the Izu-Bonin-Mariana subduction factory. In J. Eiler (Ed.), *Inside the subduction factory, Geophysical Monograph Series* (Vol. 138, pp. 175–222). Washington, DC: American Geophysical Union.
- Straub, S. M. (2003). The evolution of the Izu Bonin - Mariana volcanic arcs (NW Pacific) in terms of major element chemistry. *Geochemistry, Geophysics, Geosystems*, 4(2), 1018. <https://doi.org/10.1029/2002GC000357>
- Straub, S. M. (2008). Uniform processes of melt differentiation in the central Izu Bonin volcanic arc (NW Pacific). *Geological Society, Special Publications*, 304(1), 261–283.
- Straub, S. M. (2017). Compilation of published major and trace elements and Sr-Nd-Pb-Hf isotope ratios of Quaternary-age arc volcanic rocks from 9 arc settings. *EarthChem Library*. Retrieved from <https://doi.org/10.1594/IEDA/100664>
- Straub, S. M., Goldstein, S. L., Class, C., & Schmidt, A. (2009). Mid-ocean-ridge basalt of Indian type in the northwest Pacific Ocean basin. *Nature Geoscience*, 2, 286–289.
- Straub, S. M., Goldstein, S. L., Class, C., Schmidt, A., & Gomez-Tuena, A. (2010). Slab and Mantle Controls on the Sr-Nd-Pb-Hf Isotope Evolution of the Post 42Ma Izu-Bonin Volcanic Arc. *Journal of Petrology*, 51(5), 993–1026.
- Straub, S. M., Layne, G. D., Schmidt, A., & Langmuir, C. H. (2004). Volcanic glasses at the Izu arc volcanic front: New perspectives on fluid and sediment melt recycling in subduction zones. *Geochemistry, Geophysics, Geosystems*, 5, Q01007. <https://doi.org/10.1029/2002GC000408>
- Sulpizio, R. (2005). Three empirical methods for the calculation of distal volume of tephra-fall deposits. *Journal of Volcanology and Geothermal Research*, 145, 315–336.
- Suyehrio, K., Takahashi, N., Arie, Y., & Yokoi, Y. (1996). Continental crust, crustal underplating, and low-Q upper mantle beneath an oceanic island arc. *Science*, 272(5260), 390–392.
- Tamura, I., & Yamazaki, H. (2004). Tephrochronological study of the Hokuriku Group: The age of the Hokuriku Group by tephra stratigraphy and correlation to the widespread tephra layers. *Journal of the Geological Society of Japan*, 110, 417–436.
- Tamura, Y., Gill, J. B., Tollstrup, D., Kawabata, H., Shukuno, H., Chang, Q., . . . Tatsumi, Y. (2009). Silicic Magmas in the Izu-Bonin oceanic arc and implications for crustal evolution. *Journal of Petrology*, 50(4), 685–723.
- Tamura, Y., Tani, K., Chang, Q., Shukuno, H., Kawabata, H., Ishizuka, O., & Fiske, R. (2007). Wet and dry basalt magma evolution at Torishima Volcano, Izu-Bonin Arc, Japan: The possible role of phengite in the downgoing Slab. *Journal of Petrology*, 48(10), 1999–2031.
- Tamura, Y., Tani, K., Ishizuka, O., Chang, Q., Shukuno, H., & Fiske, R. (2005). Are arc basalts dry, wet, or both? Evidence from the Sumisu caldera volcano, Izu-Bonin arc, Japan. *Journal of Petrology*, 46(9), 1769–1803.
- Tamura, Y., & Tatsumi, Y. (2002). Remelting of an andesitic crust as a possible origin for rhyolitic magma in oceanic arcs: An example from the Izu-Bonin arc. *Journal of Petrology*, 43, 1029–1047.
- Tani, K., Fiske, R. S., Tamura, Y., Kido, Y., Naka, J., & Shukuno, H. (2008). Sumisu volcano Izu-Bonin arc Japan: Site of a silicic caldera-forming eruption from a small open-ocean island. *Bulletin of Volcanology*, 70,
- Taylor, B. (1992). Rifting and the volcanic-tectonic evolution of the Izu-Bonin-Mariana arc. In B. Taylor et al. (Eds.), *Proceedings of the Ocean Drilling Program: Scientific results* (Vol. 126). College Station, TX: Ocean Drilling Program.
- Taylor, B., Fujioka, K., Janacek, T. R., & Langmuir, C. (Eds.) (1992). *Proceedings Ocean Drilling Program: Scientific results* (Vol. 126). College Station, TX: Ocean Drilling Program.
- Taylor, R. N., & Nesbitt, R. W. (1998). Isotopic characteristics of subduction fluids in an intra-oceanic setting, Izu-Bonin Arc, Japan. *Earth and Planetary Science Letters*, 164(1), 79–98.
- Togashi, S., & Terashima, S. (1997). The behavior of gold in unaltered island arc tholeiitic rocks from Izu-Oshima, Fuji, and Osoreyama volcanic areas, Japan. *Geochimica et Cosmochimica Acta*, 61, 543–554.
- Tollstrup, D., Gill, J., Kent, A., Prinkey, D., Williams, R., Tamura, Y., & Ishizuka, O. (2010). Across-arc geochemical trends in the Izu-Bonin arc: Contributions from the subducting slab, revisited. *Geochemistry, Geophysics, Geosystems*, 11, Q01X10. <https://doi.org/10.1029/2009GC002847>
- van Achterberg, E., Ryan, C. G., Jackson, S. E., & Griffin, W. (2001). Data reduction software for LA-ICP-MS: Appendix. In P. J. Sylvester (Ed.), *Laser ablation: ICP-mass spectrometry in the earth sciences: Principles and applications, Mineralogical Association of Canada Short Course Series* (Vol. 29, pp. 239–243). Ottawa, ON: Mineralogical Association of Canada.
- Westgate, J. A., Perkins, W. T., Fuge, R., Pearce, N. J. G., & Wintle, A. G. (1994). Trace-element analysis of volcanic glass shards by laser ablation inductively coupled plasma mass spectrometry: Application to tephrochronological studies. *Applied Geochemistry*, 9, 323–335.
- Whittaker, J., Müller, R., Leitchenkov, G., Stagg, H., Sdrolias, M., Gaina, C., & Goncharov, A. (2007). Major Australian-Antarctic plate reorganization at Hawaiian-Emperor bend time. *Science*, 318(5847), 83–86.
- Wu, J., Suppe, J., Lu, R., & Kanda, R. (2016). Philippine Sea and East Asian plate tectonics since 52 Ma constrained by new subducted slab reconstruction methods. *Journal of Geophysical Research: Solid Earth*, 121, 4670–4741. <https://doi.org/10.1002/2016JB012923>
- Yamamoto, T. (1992). Chronology of the late Miocene-Pleistocene caldera volcanoes in the Aizu district, northeast Japan. *Journal of the Geological Society of Japan*, 98, 21–38.
- Yamamoto, T. (2009). Sedimentary processes caused by felsic caldera-forming volcanism in the Late Miocene to Early Pliocene intra-arc Aizu basin, NE Japan arc. *Sedimentary Geology*, 220(3), 337–348.
- Yamazaki, T., & Stern, R. J. (1997). Topography and magnetic vector anomalies in the Mariana Trough. *JAMSTEC Journal of Deep Sea Research*, 13, 31–45.
- Yuasa, M. (1995). Myojin Knoll, Izu-Ogasawara arc: Submersible study of submarine pumice volcano. *Bulletin of the Volcanological Society of Japan*, 40, 277–284.